# Metal-organic frameworks as a good platform for the fabrication of multi-metal nanomaterials: design strategies, electrocatalytic applications and prospective

Yangzhuo He [a, 1], Zhuo Yin [b, 1], Ziwei Wang [a], Han Wang [a], Weiping Xiong [a], Biao Song [a], Hong Qin [a], Piao Xu [a, *], Guangming Zeng [a, b, *]

[a] College of Environmental Science and Engineering and Key Laboratory of Environmental Biology and Pollution Control (Ministry of Education), Hunan University, Changsha 410082, P.R. China;

[b] Department of Urology, Second Xiangya Hospital, Central South University, Changsha 410011, P R China.

[*] Corresponding Authors at: College of Environmental Science and Engineering, Hunan University, Changsha 410082, PR China; E-mail addresses: piaoxu@hnu.edu.cn (P. Xu) and zgming@hnu.edu.cn (G. Zeng).

[1] These authors contribute equally to this article.

**Abstract:** MOF-derived multi-metal nanomaterials are attracting numerous attentions in widespread applications such as catalysis, sensors, energy storage and conversion, and environmental remediation. Compared to the monometallic counterparts, the presence of foreign metal is expected to bring new physicochemical properties, thus exhibiting synergistic effect for enhanced performance. MOFs have been proved as a good platform for the fabrication of polymetallic nanomaterials with requisite features. Herein, various design strategies related to constructing multi-metallic nanomaterials from MOFs are summarized for the first time, involving metal nodal substitution, seed epitaxial growth, ion-exchange strategy, guest species encapsulation, solution impregnation and combination with extraneous substrate. Afterwards, the recent advances of multi-metallic nanomaterials for electrocatalytic applications, including oxygen reduction reaction (ORR), oxygen evolution reaction (OER) and hydrogen evolution reaction (HER), are systematically discussed. Finally, a personal outlook on the future trends and challenges are also presented with hope to enlighten deeper understanding and new thoughts for the development of multi-metal nanomaterials from MOFs.

**Keywords:** Metal–organic frameworks; Derivatives; Multi-metallic nanomaterials; Electrocatalysis

## Contents

## 1. Introduction

With the depletion of fossil energy and the growing population, exploring new sustainable energy with low environmental impact has been considered as an extremely urgent and important task [1-5]. Free energy such as solar, wind, tidal and hydroelectricity are renewable, green and safe; whereas, these energies are changeable and unreliable because they are great dependence on the terrain and weather conditions. Also, these energy sources are intermittent and difficult to be gathered or released as needed, especially for solar, wind and hydroelectricity [6-8]. Utilizing energy-conversation technologies are essential for the development of energy resource. Electrocatalysis is considered as one of the most promising approaches to relieve the contemporary seriously energetic dilemma. The electrocatalytic processes refer several energy devices like fuel cell, metal-air batteries and water splitting [9-11]. Fundamentally, these technologies or devices involve different energy-conversion reactions, including the oxygen reduction reaction (ORR), oxygen evolution reaction (OER) and hydrogen evolution reaction (HER), which produce energy via directly converting chemical energy into electrical energy, or reserve energy vice versa [12, 13].

Up to now, noble-metal-based materials show excellent performance for various kinds of electrochemical reactions. As is well-known, these precious metals are expensive and scarce, which does not meet the criteria for large-scale commercialization [14-16]. Besides, when exposed to a series of chemical compounds (e.g., $CH_4$, CO, etc.), noble metal catalysts may give rise to the issues of poisoning, resulting in a greatly loss of activity [17, 18]. To overcome these problems, seeking novel electrocatalysts to replace precious-metal-based materials has received increasing attention. Over the past decades, polymetallic catalysts have attracted world-wide research interests due to their strong cooperation effects between different components. In principle, designing an ideal electrocatalyst need to consider many fundamental features like catalytic activity, electrochemical conductivity, durability, robustness and cost. However, using traditional metal salts as precursors is difficult to control the composition, surface area, and porosity. Fortunately, the discovery of metal-organic frameworks (MOFs) provides a brilliant opportunity to facilitate the multi-metal catalyst synthesis with desirable properties.

MOFs, or called porous coordination polymers (PCPs), comprising of metal ions/clusters as "nodes" joined together with organic ligands/linkers as "bridges", are a kind of highly crystalline porous materials with periodic structural units. Until now, more than 70,000 MOFs have been evolved [19], while the narrow choices of MOFs caused by their instability in water and weak conductivity restrict their further application [20-22]. Along with the phenomenal successes of MOF-related materials, MOF-derived nanomaterials have sprung up in light of their inherited morphology, ultrahigh pore volume and surface area as well as high tunability in textural characteristics [23-25]. Their promising potential has been manifested in the areas of gas sorption and storage, energy transfer, chemical catalysis and environmental remediation [26-31]. Particularly, electrocatalysis is becoming one of the most promising applications for MOF derivatives [32-36]. Utilizing MOFs as templates/precursors is an attracting route to fabricate polymetallic electrocatalysts. The precise atoms arrangement of MOF precursors enables the multi-metal catalysts with uniform distribution of the metal species, leading to powerful interaction between diverse metals [37, 38].

It is worth pointing out that several excellent reviews about MOF derivatives in electrocatalysis have been published, but they mainly focus on MOF-derived carbonaceous materials [39-41]. Multi-metallic nanomaterials as promising functional materials have shown great potential in many fields as a consequence of their unique physicochemical properties. The strong synergistic effects between metal species in multi-metallic nanomaterials give rise to enhanced performance than monometallic counterparts. On the other hand, the large diversity of metal combinations offers both design flexibility and potential for developments, significantly expanding the toolbox for the construction of desirable structured nanomaterials. Although the rapid development in this field, the exploitation of MOF-derived metal-based components, particularly multi-metal nanostructured materials is still inadequate. A timely review with emphasis on the general and effective strategies towards design, synthesis and utilization of MOF derivatives has far-reaching significance. In this review, the design strategies involved in MOF-derived multi-metal nanomaterials are first summarized and broadly falls into six categories, including metal nodal substitution, seed epitaxial growth, ion-exchange strategy, guest species encapsulation, solution impregnation and combination with extraneous substrates. Afterwards, the electrocatalytic applications of these materials as electrocatalysts in OER, ORR and HER are discussed. To close, some challenges and personal insights related to the fabrication and applications of these functional materials are proposed. This review is expected to trigger strong inspiration and provides research opportunities for further development of improved MOF-derived multi-metal nanomaterials in the field of electrochemical energy-conversion, and extended applications in electrochemistry, coordination chemistry and environmental protection.

## 2. MOFs as precursors for multi-metal nanomaterials

The derivation of MOFs emerged as a class of fascinating nanoporous materials are deeply appealing for the current research interests due to their exceptional features. The metal center in MOFs are typically transitional and lanthanide metal ions (e.g., $Mn^{2+}$, $Fe^{3+}$, $Co^{3+}$, $Eu^{3+}$, $Tb^{3+}$, etc.) and the linkers are generally organic oxygen or nitrogen-rich components (e.g., azoles, imidazoles, pyrazolates, carboxylates, etc.) [42-45]. In general, MOFs can be converted into metallic components and carbonaceous materials simultaneously, and the formed metal nanoparticles are uniformly distributed in carbon skeletons, which has been regarded as a grand challenge using other methods. It deserves to be pointed out that the successful fabrication for MOF-derived multi-metal nanomaterials highly depends on the bond breaking of the parent MOF structures. The thermal treatment and solvothermal method are usually used for preparing various MOF-derived metal-based materials [46-48]. From the perspective of synthesis, though traditional preparation methods using co-precipitation, sol-gel, combustion and impregnation are implemented economically on commercial scales [49, 50], some shortcomings still remain visible in most cases, including non-uniform distribution of metal species, lacking in pores, sintering and decrease of surface area [51-55]. For example, $CuFe_2O_{4MOF}$ catalyst prepared by MOF-templated method possessed higher Brunauer-Emmett-Teller (BET) surface area, pore volume and crystallinity than those synthesized using hydrothermal process and sol-gel combustion method, leading to more exposure active sites and stable activity [56]. Similarly, the Co/Fe Matérial Institut Lavoisier (MIL)-derived $CoFe_2O_4$ catalyst showed better catalytic activity than that obtained from conventional one-step hydrothermal method [57]. Developing MOFs as platform for preparation of polymetallic electrocatalysts is favorable. Since the electrocatalytic performance closely correlates with material physicochemical properties, synthesizing target electrocatalyst with specific properties through tailoring compositions, morphologies, and structures is of great concern [58].

Using MOFs as precursors/templates to synthesize multi-metallic electrocatalysts have many advantages (Fig. 1): (i) the well-dispersed active species owing to the intrinsic topology of MOFs even with the integration of different metal ions; (ii) the feasible introduction of heteroatoms with different electronegativity (such as N, S, P, B, etc.) to modify the electronic structure; (iii) precise regulation of metal proportion and micro-morphology by controlling the reactant ratio and themolysis conditions (e.g., heating rate, pyrolysis temperature and time); (vi) the preserved porous structure and high surface area of pristine MOFs endowing abundant cavities and channels; (v) prevention of metal migration/aggregation due to the confined effect of MOF skeleton [59-63]. Based on above considerations, selecting MOF as platform for fabrication of efficient electrocatalyst is an attracting approach.

Indeed, MOF-derived monometallic compounds possess meagre activity in certain reactions, and thus developing polymetallic catalysts seems to be an exciting way to achieve a great improvement in performance (Fig. 2) [64, 65]. Multi-metal systems have been used to optimize the adsorption energy, electrical conductivity and stability of catalysts, or to reduce the usage of precious metal maintaining the catalytic activity. The secondary metal introduced into the MOF crystal lattices could markedly facilitate charge transfer between diverse ions as well as modulate the electronic structure and surface atomic coordination [66-69]. Based on the theoretical studies, foreign metals have two primary effects on the electronic structure: the ligand effect and the strain effect [70-72]. The former refers to the perturbations of the electronic structure induced by charge transfer between neighboring metals. The later originates from variations in the lattice parameters on the surface. The introduction of secondary metal would tune the lattice parameters and thus the overlap degree between atomic orbitals, further affecting the electronic structure. Both effects are generally inseparable and collectively lead to the modified electronic structure. On the other hand, the secondary metal ions could serve as a geometrical spacer to spatially insulate other metal species [73, 74]. Taking a rod-like NiS/ZnOS as an example [75], the Zn species existed in parent MOFs serve as geometrical spacer between Ni to restrain its sintering, leading to the formation of smaller NiS and thus benefiting the creation of abundant active sites as well as the decrease of activation energy for hydrogen reduction. In another case, the introduction of $Mg^{2+}$ in MgNi-MOF-74 helped to realize spatial separation of $Ni^{2+}$ in M-oxo chains, resulting in the formation of single-atom Ni. With these intriguing merits in mind, multi-metal electrocatalysts starting from MOFs has aroused intense attention worldwide. Fig. 3 summarized the development milestones of MOFs and MOF-based polymetallic nanomaterials used for electrocatalytic applications.

The good strategy and fabrication of multi-metallic nanomaterials derived from MOFs is important for a better understanding of the structure-property relationship. The most crucial factor in the activity of these nanomaterials depends on morphology that includes shape, size, arrangement and structure. Particularly, the nanostructures materials with large surface area, numerous active sites, hierarchical pores, uniform doping and high conductivity are beneficial to achieve superior electrocatalytic performance. Through self-templating approach, the derivative's morphology is mainly inherited from the parent MOF owing to the sufficient thermal stability. Nevertheless, for the synthesis by an external-templating method, various morphologies could be obtained by calcining the combination of MOFs and templates.

Previous studies reported that the reaction conditions such as temperature, organic solvent and metal content also significantly affect the sample morphology [76-78].

In general, these nanomaterials in terms of morphology could be classified as: 0D (polyhedrons, hollow and core-shell structures), 1D (nanotubes and nanorods), 2D (nanoflakes, nanoplates and nanofilms), and 3D (foams, flowers and honeycomb like frameworks). Polyhedrons including dodecahedrons, hexahedrons and octahedrons are the most prominent and well-studied structures. Typically, ZIF precursors that have many edges and corners are frequently utilized to produce this type of nanostructures with numerous accessible active sites [79]. Hollow nanomaterials are characteristic of large surface areas, high loading capacities and low densities compared to their solid counterparts. Core-shell structures are able to provide good dispensability, functionality and stability [80]. Mostly, pre-designed core-shell MOF precursors are applied for the preparation of these nanostructures. By seed epitaxial growth method, hollow/core-shell structure can be easily obtained. 1D nanostructures with certain features same as 0D and 2D materials have different properties from bulk materials, such as mechanical, electronic and optical property [81, 82]. For the synthesis of 1D nanomaterials via self-templating method, there are few 1D MOF precursors are available. The large surface area of 2D nanomaterials enable them possess more exposed active centers, as compared to bulk materials. MOF precursors with lamellar morphology are usually used for the fabrication of 2D nanostructures via self-templating approach [83, 84]. By combining MOFs with flexible substrates, 3D nanomaterials with versatile morphologies can be achieved, such as foams, sponges and flowers like frameworks. Compared to lower-dimension nanomaterials, 3D nanostructures with interconnected networks have larger accessible surface area. Benefiting from the spatial arrangement of particles in 3D framework, nanomaterials acquire the tunable host-guest interactions, size-selective properties and surface functionalities, leading to an enhancement of overall electrochemical activity and stability [85, 86].

## 3. Design of multi-metallic nanomaterials from MOFs

As is well-known, MOFs are constructed through organic ligands coordinated with metal nodes. Their highly flexibility in topological structure and composition make them as suitable platform to fabricate multi-metal nanomaterials with excellent performance. In this section, six primary strategies in reference to the construction of multi-metallic nanomaterials from MOFs are systematically discussed for the first time, including metal nodal substitution, seed epitaxial growth, ion-exchange strategy, guest species encapsulation, solution impregnation and combination with extraneous substrates (Fig. 4). In some cases, these methods are utilized simultaneously. The advantages and disadvantages of these strategies have been summarized in Table 1.

### 3.1. Metal nodal substitution strategy

Metal nodal substitution refers to incorporation of the foreign metal species with similar ionic radii of the metals into host framework crystal lattice [87, 88]. This popular strategy is regarded as the most straightforward method for the preparation of mixed metal nanomaterials due to its prominent features. Specifically, the facile substitution of metal nodes using one-pot reaction, i.e., different metal ions and linkers are simultaneously dissolved in organic solvent or water and then followed by self-assembly process to obtain target products, can retain the original MOF crystal structure without obvious destroy. In this process, the metal ions come from both soluble salts and metal foils (e.g., copper foils).

The usage of different metal salts in MOF synthesis shows great impact on the particle sizes ranging from the nanoscale to microscale. In the work of Torad, nano-sized zeolitic imidazolate framework-8 (ZIF-8) crystals with an average size of 50 nm were prepared when $Zn(NO_3)_2$ was utilized as zinc source [89]. Owing to the weak solvation of $Zn^{2+}$ ions in methanol solution, the $Zn^{2+}$ ions could coordinate with 2-methylimidazole (2-MIM) easily, thus leading to the rapid generation speed of ZIF-8 with small size. While the particle size was increased to 2 μm when $Zn(NO_3)_2$ replaced with $Zn(CH_3COO)_2$. This could be put down to the strong interaction between the dissolved $Zn^{2+}$ ions and $(CH_3COO)^-$ ions along with the solvation of $Zn^{2+}$ ions, which drastically slowed down the nucleation.

It is noteworthy that some specific agents such as poly(vinylpyrrolidone) (PVP), cetyltrimethylammonium bromide (CTAB) and sodium dodecyl sulfate (SDS) are usually employed for the surface modification in the synthesis process [90-92]. Nanoparticles with various size, shape and composition can be fully confined and well dispersed inside MOF matrix with the help of surfactant [93-95]. In Pan's work, ZIF-8 showed a typical rhombic dodecahedron with the mean particle size of 4 μm without CTAB addition [96]. When the CTAB contents in the MOF synthesis solution increased from 0.0025 wt% to 0.025 wt%, the morphology of ZIF-8 gradually changed from truncated rhombic dodecahedron to truncated cubes and the size continually decreased from 2.8 μm to 110 nm, in which the long hydrocarbon chains play a vital role in changing the shape and the MOFs size. Similar phenomena also were observed by using cetyltrimethylammonium chloride (CTAC) and trimethylstearylammonium chloride (STAC). Zhan and co-workers reported the surfactant-induced amorphization of ZIF-90 (Fig. 5a) with a random network topology instead of the sodalite topology (Fig. 5b) [97]. Monocrystalline ZIF-90 with rhombic dodecahedral shape can be obtained by mixing zinc salts and imidazole-2-carboxaldehyde directly. After the addition of CTAC surfactant in the synthetic solution, $a_m$ZIF-90 with hierarchical dandelion-like morphology composed of many radially distributed nanorods as its building blocks was produced (Fig. 5c, d). Aside from the CTAC, other surfactants such as anionic surfactants (SDS) and cationic surfactants (CTAB, and dodecyltrimethylammonium bromide, DTAB) were also studied in their work. $a_m$ZIF-90 with similar rodlike building units and their assemblies was yielded by both cationic surfactants (Fig. 5e, f). Using DTAB could obtain the pure $a_m$ZIF-90, while a small number of crystalline ZIF-90 was also generated when CTAB was utilized (Fig. 5g).

Copper foil recently is exploited for synthesis of polymetallic ZIF precursors containing $Fe^{2+}$ by a simple redox reaction (i.e., $2Fe^{3+} + Cu = Cu^{2+} + 2Fe^{2+}$). The adoption of copper foil to obtain mixed metal MOFs are not only able to introduce the Cu species with high activity, but also prevent the $Fe^{2+}$ from oxidation during the growth of MOFs. Generally, $Fe^{2+}$ is more favorable to achieve uniform Fe doping in ZIF-8 scaffolds compared with $Fe^{3+}$ because of the severe structural distortion with $Zn^{2+}$ substitution by $Fe^{3+}$ [98]. Whereas, Fe doped ZIFs should be synthesized under an oxygen-free environment to avoid the transformation of $Fe^{2+}$ to $Fe^{3+}$, which makes the operation process more complicated and cumbersome [98, 99].

Using copper foil as Cu source and reductant, Wang and co-workers prepared Fe, Cu-coordinated ZIF-derived Cu@Fe-N-C by thermal treatment in Ar gas (Fig. 6a) [100]. The color change of solution from yellow to light green verified the successful synthesis. The introduced Fe and Cu ions in zinc-based MOFs gave rise to a morphological variation and great increase of MOF size due to partial deprotonation of organic ligands and extended growth directions in the existence of $Cu^{2+}$ and $Fe^{2+}$. The homogenous distribution of Cu and Fe species throughout the entire architecture was clearly discerned from the elemental mapping (Fig. 6b). Through the same reaction process, Zhang et al. developed multi-metal (Fe, Cu, Zn, and Co) mixed ZIF by a one-pot procedure of an in situ ionic reaction in the ambient atmosphere (Fig. 6c) [101]. Copper foil was immersed into the solution having $Zn^{2+}$, $Co^{2+}$ and $Fe^{3+}$ ions to yield $Cu^{2+}$ and $Fe^{2+}$. After calcination, an exceptionally porous carbon polyhedron

(FC-C@NC) grafted with plentiful carbon nanotubes (CNTs) were synthesized (Fig. 6d). The ultrafine Co NPs with lattice sites partly substituted by Cu and Fe were embedded into the resultant FC-C@NC (Fig. 6e). The obtained FC-C@NC nanomaterials were characteristic by large surface area, highly porous structure, active metal sites and conductive carbon frameworks, contributing to outstanding ORR activity. Without the addition of copper foil, Fe-CoZn-ZIF was failed to directly prepare at the same conditions by a co-precipitation method in the solution containing $Fe^{2+}$ (Fig. 6f). These works pave a way for efficient and convenient design of Cu-assisted generation of $Fe^{2+}$ during the MOF-growth.

Using metal nodal substitution strategy through a one-pot process is believed to be a facile and usual route for preparation of mixed metal nanomaterials. Various metal salts coordinated with organic linkers in a homogeneous solution, in which surfactants also can be used to functionalize MOFs, making it easy to control the particle size, morphology and chemical composition. The coordination environment provided by MOF ligands helps to adjust the dispersion of metal active sites by the selective change of MOF nodes and the incorporation of other metals. Moreover, the doped metals can be selectively removed. The original structure of MOFs can be preserved well owing to the lattice substitution of metal dopant. On the other hand, the simple but effective modulation of metal content in MOF scaffold also can be realized by changing the ratio of metal salt precursors. Whereas, those metal ions with large differences in electronic configuration are still difficult to be doped into the metal host frameworks, stemming from their difference in coordination behavior with organic ligands.

### 3.2. Seed epitaxial growth strategy

Seed epitaxial growth is an efficient method to fabricate dual-MOF core-shell structures [102-105]. Owing to their similar crystal structure and lattice constant, the MOF shell epitaxially grown on another MOF seed can be successfully achieved. Using such strategy, the advantages of MOFs can be incorporated fully to generate significant synergistic effects [106]. Early in 2014, Huang et al. reported core-shell $Co_3[Fe(CN)_6]_2@Ni_3[Co(CN)_6]_2$ nanocubes using PBA as starting materials [107]. Specifically, NiCo PBA as seed was fabricated by co-precipitation method in the aqueous mixture of $NiCl_2 \cdot 6H_2O$ and $K_3[Co(CN)_6]$. In light of the similar crystal structure and unit cell parameter, a layer of CoFe PBA was epitaxially deposited onto the surface of NiCo PBA nanocubes to form a core-shell CoFe@NiCo precursor. During MOF epitaxial growth, sodium citrate as an additive interacted with the metal ions in the homogeneous solution to decrease the coordination rate between the ligands and metal ions. Later on, the same group proposed another study by using core-shell $Fe_2Ni$ MIL-88/Fe MIL-88 as templates [108]. The dual-MILs nanorods were successfully fabricated through consecutive hydrothermal reaction of Fe MIL-88 precursors in the solution containing initially formed $Fe_2Ni$ MIL-88 seeds. Then, core-shell MILs were converted into the final $NiFe_2O_4/Fe_2O_3$ nanotubes by a post-annealing process. Huang et al. developed a facile method to fabricate $CoFe_2O_4/CuO$

(sub)microcages using dual-MOF $Fe^{II}$-Co PBAs@HKUST-1 heterostructures as both the precursor and self-sacrificing template [109]. $Fe^{II}$-Co PBAs were first prepared and then used as seeds to synthetic core-shell $Fe^{II}$-Co PBAs@HKUST-1 crystals. After thermal annealing in air, $Fe^{II}$-Co PBAs@HKUST-1 composites were chemically transformed into $CoFe_2O_4/CuO$ (sub)microcages, which effectively retained the morphology and porous structure of original MOFs, synchronously achieving homogeneous heteroatom doping and unique hollow architecture.

In Aslam's work, time dependent ZIF-67@ZIF-8/ZIF-67 nanoparticles were prepared by the kinetically controlled synthesis and then converted to hollow ZnCoS@$Co_9S_8$/NC (Fig. 7a) after sulfidation and calcination [110]. Cobalt precursors were added into the solution of 2-MIM ligands and the homogeneous solution transformed from transparent to turbid over time. After 7 minutes, Zn salts were dissolved in the above mixed solution to afford the bi-metallic Co-to-Zn nanoparticles. The edge growth of inside ZIF-67 crystal and outside ZIF-8/ZIF-67 structure was clearly confirmed by field emission scanning electron microscope (SEM) (Fig. 7b-c). Through sulfidation and pyrolysis process, ZIF-67@ZIF-8/ZIF-67 was evolved to yolk-shelled ZnCoS@CoS and further converted to single-holed hollow ZnCoS@$Co_9S_8$/N-doped carbon with core-shell structure. The N-doped porous carbon endowed the catalyst with fast electron transport to achieve exceptionally high-rate capability. Huang et al. fabricated $MoC_2$/Co embedded hybrid hollow N-doped carbon polyhedrons (CoMo@HNCP) using core-shell ZIF-8@HZIF-CoMo as precursors

(Fig. 7d-h) [111]. In the presence of PVP, the as-prepared ZIF-8 microcrystals as seeds reacted with Co ions, $H_2MoO_4$ and organic ligands to form polymetallic core-shell architecture. By further annealing under $N_2$ atmosphere, the target CoMo@HNCP were obtained. Benefiting from the homogeneous distribution of metallic Co and $Mo_2C$ NPs in the hollow N-doped carbon shell, the produced multiple heterogeneous interfaces helped to improved performance, making it superior to that of ZIF-8 derived N-doped carbon and HZIF-CoMo derived bimetallic carbon polyhedron. Undesirably, the reaction of HZIF-CoMo shell growth on ZIF-8 core are time-consuming and power-wasting, which limited this method for further utilization and large-scale production in industry.

The polyhedral core-shelled MOF architecture can be facilely fabricated by using seed epitaxial growth strategy. After heat treatment, the core-shell/hollow nanomaterials are usually obtained, and the integrity of parent MOF is able to retain to a great extent. Compared to the single MOF crystal, the combination of different types of MOF can exert complementary and synergetic effect effectively. Typically, the ZIF-67 has been well demonstrated to afford its derivate with uniform N doping, $CoN_x$ sites and high graphitization degree yet low surface area; the ZIF-8, isostructural to ZIF-67, should be a suitable candidate because it can offer derivate with high surface area and porosity. Thus, the bimetallic ZIFs based on ZIF-8 and ZIF-67 are expected to inherit both merits of derivates independently from separate ZIF. Whereas the requirement of similar topological structure restricts its wide application. During synthetic process, the precise operation (e.g., seed contents, metal ratio, stirring time/rate, etc.) is required to achieve the successful epitaxial growth. In these reported literatures, majority are found to be narrowly confined to ZIFs. In the future, more attempts should be paid to other types of MOFs.

### 3.3. Ion-exchange strategy

Ion-exchange is a classical solid−liquid interface reaction occurring in the solid MOF precursors and chemical reagents in the solution. The simultaneous incorporation of various materials with distinct physical-chemical properties can be achieved by using this strategy. Since the coordination bonds in MOFs between metal nodes and organic ligands are weak yet reversible, these bonds within skeleton can be easily break to prepare multivariate MOF templates with different metal centers through ion exchange process [112-114]. The well-matched ion exchange and etching process occurred at the two-phase interfacial lead to the well-retained architecture and dimensions of original MOFs. According to the different type of the exchanged chemicals, ion-exchange reaction is classified into cation-exchange reaction and exchange process involving anion.

Cation-exchange are intensively applied to introduce second metal into a single MOF framework to form mixed metal composites. For example, Co-ZIF-67 as a template was prepared first using a usual method and then reacted with $Ni(NO_3)_2 \cdot 6H_2O$ in ethanol solution to produce a Ni–Co MOF through cationic exchange reaction [115]. In this process, these released $Co^{2+}$ and partially oxidized

$Co^{3+}$ co-precipitated with $Ni^{2+}$ to produce Ni−Co MOF. The bimetal MOF precursor still preserved a polyhedral morphology yet showed a rougher surface owing to the construction of nanosheets. Followed by a subsequent annealing treatment, hollow porous $NiCo_2O_4$-nanoboxes were obtained. Xu and colleagues demonstrated a cation-exchange approach for the conversion of ZIF-67 into $Co_3O_4/TiO_2$ hollow polyhedrons [116]. Instead of using ethanol as solvent, they applied N, N-dimethyl formamide (DMF) for the $Ti^{4+}$ exchange reaction because $Co^{2+}$ ions are unable to hydrolyze in basic DMF solution, leading to the cation exchange occurred on the surface of ZIF-67. It is worth mentioning that the cationic exchange took place relied on the lower electronegativity of $Ti^{4+}$ than $Co^{2+}$. The ZIF-67 crystal was first dissolved and its bond between the $Co^{2+}$ cations and cluster was broke to re-bond with $Ti^{4+}$ cations stepwise. The DMF molecules gradually linked with Co ions since they still bounded to the cluster. Then, $Ti^{4+}$-exchanged ZIF-67 skeleton was formed via the partial replacement of $Co^{2+}$ by $Ti^{4+}$. The ZIF-67 host showed adequate stability and flexibility to accommodate these exchanged $Ti^{4+}$.

Polymetallic MOFs with single or multiple shelled nanostructures also can be fabricated by cationic exchange reaction. Starting from ZIF-67, yolk-shelled ZIF-67/Ni−Co LDHs structures were synthesized and subsequent converted them into $Co_3O_4/NiCo_2O_4$ double-shelled nanocages (DSNCs) by pyrolyzation [117]. Replacing $Ni(NO_3)_2$ by $Mg(NO_3)_2$ and $Co(NO_3)_2$, a series of single-shelled LDHs were effectively constructed, including ZIF-67/Mg−Co LDHs and ZIF-67/Co−Co LDHs, suggesting a strong universality of this strategy. In reference to similar route, the same group developed double-shelled $Co(OH)_2$@NiCo-LDH nanocages from single-shelled ZIF-67@LDH [118]. During this process, $Na_2MoO_4$ was utilized to generate $OH^-$ ions through hydrolysis, and then $OH^-$ precipitated with $Co^{2+}$ to yield $Co(OH)_2$ shell. Importantly, the as-prepared products maintained the polyhedral shape of parent ZIF-67 core.

Additionally, anion-exchange reaction is also widely studied for the fabrication of novel-structured MOF hybrids. A series of multi-compositional microboxes reported by Lou et al. represented a good example [119]. Using microsized Prussian blue (PB) ($Fe_4[Fe(CN)_6]_3$) crystals as templates and $K_2SnO_3$ as secondary metal source, hollow $Fe(OH)_3/SnO_2\cdot xH_2O$ were synthesized via the ion exchange coupled with the hydrolysis reaction. $K_2SnO_3$ as conjugate base partially hydrolyzed to form oxide hydrate and created a proper alkaline environment, which induced PB cubes converted to $Fe(OH)_3$ microboxes through $OH^-$ ions exchanged with $Fe(CN)_6^{4-}$. Meanwhile, the in situ and stoichiometric precipitation of $SnO_2\cdot xH_2O$ was facilitated by the consumption of $OH^-$ during the generation of $Fe(OH)_3$ shell, giving rise to the formation of $Fe(OH)_3/SnO_2\cdot xH_2O$ precursors. By annealing treatment of the as-prepared samples, $Fe_2O_3/SnO_2$ microboxes were produced. Using $Na_2GeO_3$ and $Na_2SiO_3$ as the alkaline precursors, $Fe_2O_3/SiO_2$ and $Fe_2O_3/GeO_2$ microboxes were acquired based on the same approach. In another work, $Na_2MO_4$ (M = Mo or W) was selected as alkaline precursors for the synthesis of $CoMO_4$–$Co(OH)_2$ nanocages [120].

At the first 20 min, the color change of solution implied the initiation of reaction between $MoO_4^{2-}$ and solid ZIF-67. When the refluxing time prolonged to 2 h, hollow $CoMoO_4$–$Co(OH)_2$ nanocages were fabricated. Chen et al. reported an anion-exchange modification to synthesize Fe doped cationic Co(II)-based MOF and then transformed into Fe-Co-N-C catalysts, where the $ClO_4^-$ anions with charge balance blocked into its one-dimensional (1D) channels [121]. Through exchanging with $ClO_4^-$ anions, $[Fe(CN)_6]_3^-$ anions generated from $K_3[Fe(CN)_6]$ were introduced into the MOF channels, resulting in the formation of Fe/Co-coexisting MOF. After ion-exchange process, the integrity of MOF scaffold preserved well. Owing to the $[Fe(CN)_6]_3^-$ decomposition and the catalytic role of Fe atoms, Co NPs were wrapped by graphitic carbon layers, which were confirmed as one type of active sites for ORR.

Furthermore, the reactant concentration in the exchanged system has a remarkable effect on the composition and shell number. For instance, Lou and co-workers demonstrated a conversion of ZIF-67 into ZIF-67@amorphous-$Co_3V_2O_8$ structure with the vanadium oxytriisopropoxide (VOT) as vanadium source [122]. Through an anion-exchange reaction, 2-MIM anion in ZIF-67 skeleton was stepwise replaced by the $VO_4^{3-}$ from VOT to generate amorphous $Co_3V_2O_8$ shell. Particularly, the yolk-shelled ZIF-67@amorphous-$Co_3V_2O_8$-50 with a thin shell and a large ZIF-67 core were obtained at 50 μL VOT amount. When the VOT concentration increased to 70 μL, a similar yolk–shelled structure with a thicker shell and a shrunken core can be observed. As the VOT amount further increased to 120 μL, the ZIF-67 core was entirely consumed to form hollow amorphous-$Co_3V_2O_8$ nanoboxes. Accordingly, $Co_3O_4$@$Co_3V_2O_8$ nanoboxes with triple shell and double shell and single-shelled $Co_3V_2O_8$ were separately acquired after thermal annealing in air.

Ion-exchange strategy, as an energy-saving procedure, usually takes place at mild conditions. This method can form uniform nanocomposites in situ, which not only protects the original MOF structures from damage but also is scalable for large-scale production. For time-consuming exchange process (usually more than 24 h), microwave-assisted synthesis could be considered for rapid synthesis. Of note, the electronegativity of metal ions plays important role in the ion-exchange reaction. Through ion-exchange process, multiple shelled structures can be facilely obtained from solid precursors and simple-component can also be converted into multiple-component composites. Hence, the ion-exchange reaction may create great opportunity to fabricate complex nanomaterials in the light of both shell architecture and chemical composition. During the etching process, the concentration of exchanged substance is of great importance for the final morphology of polymetallic materials, further affecting their performance in reaction system. Notably, the structural distortion may occur due to the inappropriate exchanged time.

### 3.4. Guest species encapsulation strategy

The cavities in MOF skeletons endow them with adequate space to accommodate the naturally incompatible metal species, which can function as ideal platform for the preparation of multi-metallic guest@MOF precursors with new fascinating properties

[123-125], whereas, it is difficult to perform by conventional methods. The rational immobilization of metal-containing species inside the MOF voids can purposely design functional nanomaterials with new fascinating properties. For example, Wang and co-workers reported a facile double-phase encapsulation approach (DPEA) to synthesize NiCoTU@$NH_2$-MIL-101(Al) co-precursors (Fig. 8a) [15]. Herein, $NH_2$-MIL-101(Al) with large pores (ca. 2.9 and 3.4 nm) was chosen as host template for the accommodation of Ni-Co coordination compound and thiourea (TU). Benefiting from the immiscibility of the hydrophilic water-ethanol solution containing Ni-Co/TU and hydrophobic solvent of *n*-hexane, the as-proposed DPEA enabled the direct incorporation of the guest species into the internal pores of MOF template suspended in *n*-hexane. Subsequently, a heat treatment was carried out to prepare the Ni-Co-S@G/NSC samples. The encapsulation of the Ni-Co precursors and their uniform 3D distribution within the $NH_2$-MIL-101(Al) were conducive to forming small Ni-Co-S NPs and simultaneously induce the N and S active sites, resulting in excellent electrocatalytic activity. Similarly, $Ni(NO_3)_2$ and $Cu(NO_3)_2$ mixed solution were dropwise pumped into the suspended MIL-101(Cr) with hexane as solvent [126]. Then, the $Cu^{2+}$ and $Ni^{2+}$ ions encapsulated into MIL-101(Cr) pores were reduced by $NH_3BH_3$ to afford CuNi@MIL-101(Cr). During this process, Cu NPs were formed first and served as seeds to trigger the followed reduction of $Ni^{2+}$ ions to produce CuNi NPs.

The integration of noble metal NPs into MOF pore channels and then calcinated at high temperature can afford the alloy structure, which not only gives a considerable enhancements for the physicochemical properties but also improves the utilization efficiency of noble metals [127]. For instance, Pt@ZIF-67 were prepared based on the hydrophobic/hydrophilic method [128]. Specifically, ZIF-67 with hydrophilic nature first dispersed in a hydrophobic solvent of *n*-hexane, and then Pt NPs were adsorbed into the MOF pores owing to its hydrophilic affinity towards ZIF-67. Followed by hydrogen reduction and covered with tannic acid (TA), Pt@ZIF-67@TA precursors were produced. After pyrolysis, the final PtCo/Co@NHPCC catalysts were obtained, where the unique alloy structure and ultrafine PtCo NPs improved the inherent activity, stability as well as utilization efficiency of Pt. The hollow porous carbon support with nitrogen dopant and high surface area was contributed to the excellent catalytic property. The concentration of solvent is important in the synthetic procedure. A mass of *n*-hexane was help to disperse ZIF-67 particles and generate the repulsive outer hydrophobic environment around Co-ZIF, promoting the adsorption process of metal precursors. Recently, the Au and Pd ions guests were trapped into ZIF-67 pores by a *de novo* method, followed by reduction into bimetallic Au-Pd NPs in $NaBH_4$ solution [129]. A further thermal treatment under air was employed to yield $Au_xPd@Co_3O_4$ cages with an active interface between cobalt oxide and Au-Pd alloyed NPs (Fig. 8b-d). In this work, ZIF-67 served as a template to separate cobalt clusters while not catalyst. The organic ligands in ZIF-67 were sacrificed to make the $Co^{2+}$

ions close, leading to the formation of the efficient interface with powerful interaction. It is noting that Au and Pd tended to form bimetallic NPs instead of alloy NPs after reduction process because both two noble metals possessed multiple oxidation states in the AuPd@ZIF-67 composites.

Aside from metal NPs, polyoxometalates (POMs) are widely utilized to encapsulate into MOF pores to construct guest@host template. POMs are a class of metal-oxygen anion clusters abounding in transition metal source (e.g., Mo, W, V), which have emerged as promising precursors to synthesize the active Mo- or W-containing catalysts. MOFs embedded with POMs endow the composites with greatly enhancement in performance owing to the combination of individual advantages [130, 131]. As an example, Li et al. conceived an effective strategy to design $PMo_{12}$-incorporated MIL-100 (Fe) precursors, which responsible for the source of Fe, Mo and P simultaneously [132]. In the mixture of $H_3PMo_{12}O_{40}$, Fe salts and organic linkers, $PMo_{12}$ was formed accompanied with the self-assembly process of MIL-100 (Fe). This method simplified the synthetic procedures and reduced the energy consumption. The obtained $PMo_{12}$@MIL-100 (Fe) showed polyhedral morphology, similar to parent MIL-100 (Fe), suggesting the structure still maintained intact after encapsulated operation. Followed by calcination with melamine, $Fe_3C/Mo_2C$-containing N, P co-doped graphitic carbon was obtained (Fig. 8e). Without the addition of $PMo_{12}$, sole MIL-100 (Fe) derived $Fe_3C$@C exhibited a lower graphitic degree than that of $Fe_3C/Mo_2C$@NPGC (Fig. 8f, g). In another case, Tang and co-workers demonstrated a novel solid-phase hot-pressing method to fabricate POMs-based Co/Zn-ZIFs precursors on carbon cloth (CC) without the usage of binders [133]. In brief, $PMo_{12}$, $Zn^{2+}$ ions, $Co^{2+}$ ions, organic ligands and polyethylene glycol with a little ethylene glycol were grinded together to produce purple pastes. Later, the pastes were deposited on CC using an electric iron at moderate environment to form $PMo_{12}$-Co/Zn-ZIFs/CC composites. Subsequently, the CoP/MoP@NC/CC with unique structure and large surface area was prepared through the phosphidation. Compared to the traditional solvent method, this method has many advantages of rapid synthesis, mild reaction conditions, non-pollution and high yield.

Based on the ordered porous structure of MOFs, the guest species encapsulation strategy is effectively proposed. The successful implementation of such method relies heavily on the well-matched pore size of MOF template with molecular/ion dimension. Owing to the geometric confinement effect of MOFs, guest species confined in MOFs after calcination could avoid the particle aggregation and these obtained metal NPs may be small-sized, uniformly embedded within the carbon matrix with a high density, thus showing an improved reactivity for specific application. Besides, MOF scaffolds can serve as a multi-spatial-compartmental nanoreactor that allows physically compartmentalize multiple active species in a single MOF nanoparticle for facilitating mass transportation. However, the selection of the type and content of guest species encapsulated into the MOF hole is narrow due to the intrinsic feature of pore structure of MOFs, which hindered the widespread usage of this strategy.

### 3.5. Solution impregnation strategy

Impregnation method has been widely applied in industrial field. Generally, MOF precursors are subjected to calcination and then the obtained derivatives are infiltrated by metal solution followed by post-treatment to generate the final multi-metal nanomaterials with unique properties [134]. Unlike other strategies, this synthetic method is to introduce foreign metal species into the skeletons of MOF derivatives instead of pristine MOFs. Accordingly, more meticulous operation and mild conditions are needed to avoid the structural damage.

Zhou et al. synthesized Co-Fe bimetallic composites using impregnation method with iron acetylacetonate as Fe source [135]. Starting from ZIF-67, Co/N-C dodecahedral nanocages (DNCs) were fabricated by high-temperature calcination. Then the obtained Co/N-C samples were mixed with iron acetylacetonate at 300 ℃ to produce Co-$Fe_3O_4$/N-C DNCs, in which $Fe_3O_4$ NPs grew on the inside and outside surfaces of Co/N-C. After annealing with S power, $Co_8FeS_8$/N-C DNCs were finally synthesized. The structure of $Co_8FeS_8$/N-C DNCs still remained integrity without obvious destroy after solution impregnation process and twice high-temperature calcination. The bimetallic $Co_8FeS_8$ NPs were evenly embedded within porous hollow N-doped carbon matrix, leading to the synergy effect for remarkable performance. Xu and co-workers prepared Fe-introduced Zn@Co-MOF composites by two-step method [136]. At first, a core@shell structured ZIF-8@ZIF-67 was synthesized by precise epitaxial growth. After that, guest Fe ions from iron nitrate were introduced into Zn@Co-MOFs host through wet impregnation to obtain the final samples.

Li et al. reported a general route to fabricate tri-metallic nanorods using bimetallic FeNi-MOFs as templates [137]. The bi-MOF precursors were transformed into $FeNi_3C_x$ nanorods by thermal annealing under argon atmosphere. In this process, $Fe^{2+}$ and $Ni^{2+}$ ions were reduced into alloyed FeNi NPs by the carbonaceous species came from trimesic acid ligands. The as-obtained $FeNi_3C_x$ nanorods were dipped into the aqueous solution of $Na_2PdCl_4$ to form $FeNi_3C_x$-$Pd_y$ with claviform shape. During which, $Pd^{2+}$ ions reacted with L-Ascorbic acid on the surface of $FeNi_3C_x$ nanorods, leading to the uniformed dispersion of crystalline Pd NPs on the outer carbon layer. Similarly, Cu-MOF-derived Cu/C precursor powders were slowly added into a chloroplatinate solution for 15 min to synthesize a core-shell structured Cu@Pt/C catalyst [138]. Note that, even a little amount of Cu species in Cu@Pt/C can induce more active sites to greatly improve the electrochemical activity compared to pure Pt/C. Mandegarzad et al. reported a novel catalyst based on bimetallic Cu-Pd NPs supported on nanoporous carbon composites (Cu-Pd/NPCC) through a three-step process [139]. MOF-199 ($Cu_3(BTC)_2$, BTC = 1,3,5-benzenetricarboxylate) was selected as precursor and synthesized by an electrochemical method. Further direct carbonization under $N_2$ atmosphere was performed to obtain Cu/NPCC. After the addition of $PdCl_2$ solution, Cu-Pd/NPCC was fabricated via galvanic replacement of

Cu atoms by Pd (II) ions. The Pd NPs with size of 50–90 nm were well dispersed on the porous network of the Cu/NPCC. Benefiting from the interaction effect of bimetallic composite due to diminishing of d-band center of Pd by Cu component, the catalysts showed excellent electrocatalytic activity towards HER.

Recently, Guo et al. demonstrated two routes involving one-step and post-treated method to construct $CeO_2$-based bimetal oxides [140]. In detail, $CeO_2$-CuO catalysts were synthesized by thermolysis of Ce-centered MOFs followed by loading CuO species using impregnation method. Differently, Ce-Cu-$O_x$ catalysts were obtained from the direct carbonization of bimetal Ce(Cu)-MOFs. Surprisingly, both of them presented a similar rod-like structure and pore size distribution as well as comparable surface area. However, $CeO_2$-CuO sample displayed intensively higher lattice oxygen percentage of 60.8% than that of Ce-Cu-$O_x$ of 46.0%, giving rise to superior activity in CO oxidation. The different synthetic approach led to varying synergetic interaction between $CeO_2$ and CuO species, and thereby affected the defect sites, redox ability, and $Cu^+$-CO adsorption strength. It is worth mentioning that the extremely low quality of CuO species, homogeneous dispersion and integrated into the $CeO_2$ lattice resulted in the absence of characteristic diffraction peaks of CuO in XRD pattern of $CeO_2$-CuO and Ce-Cu-$O_x$ samples.

The MOF derivatives are completely and uniformly immersed in metal-containing solution by using solution impregnation strategy. After thermal treatment, the metal NPs could homogeneously grow on the inside and outside of MOF derivatives. Although solution impregnation has been proven to be efficient, the complex and tedious operation involved multiple steps in synthesis may bring a possibility of structural failure, which could increase the cost and reduce the reproducibility of samples. It is highly significant to carefully manipulate the infiltrating reaction between MOF derivatives and foreign metal source through controlling the reaction conditions. Besides, in some cases, the slight collapse of pore structure of MOF after pyrolysis makes it difficult to immersing metal species into pores. The size compatibility between derivative and metal component is important. In the future, more wide and deep investigations along with the solution impregnation strategy are highly needed to explore facile yet efficient route to prepare multicomponent materials.

### 3.6. Combination with extraneous substrates

MOF precursors combined with extraneous pre-designed metal substrates to fabricate the multi-component materials have gathered intensive interests [141, 142]. These distinctive substrates possessing diverse morphology are deem to be favorable supports for MOFs. The formed intimate physical and chemical contact between them offers opportunity for generation of new properties [143, 144]. Although some metal component can play a role solely, the results still leave much to be desired. Integrating with functional MOF-based materials is an effective way to improve their performance. In the research of Kuang, bimetal Cu, Co-embedded N-enriched carbon matrix (CuCo@NC) catalysts were synthesized by using ZIF-67 on $Cu(OH)_2$

nanowires as co-precursors (Fig. 9a-c) [145]. ZIF-67 was in situ grown on the as-obtained $Cu(OH)_2$ nanowires through a self-assembly reaction. Then, the as-synthesized $Cu(OH)_2$@ZIF-67 composites were transformed into the final CuCo@NC by thermal treatment under inert gas at 800 ℃ followed by acid etch. The different tolerance for decomposition temperature of ZIF-67 and $Cu(OH)_2$ provided a confinement effect of Co and Cu metals within N-doped carbons, avoiding the self-aggregation and irreversible fusion of Cu NPs (Fig. 9d). Similarly, a certain amount of CuO nanosheets were inserted into the dodecahedral ZIF-8 to construct CuO-ZIF-8 composites and then evolved into Cu, Zn embedded porous carbon frameworks (CuZn@C) [146]. The CuO nanosheets were converted to small $Cu_2O$ NPs at high temperature. With the increase of CuO amounts, the BET specific surface area of CuZn@C was decreasing owing to the pore blockage of Cu species. In the research of Zhao, carbon nanotube fibers (CNTFs) were mixed with $Zn^{2+}$ and $Co^{2+}$ solution for the preparation of $ZnCo_2O_4$ nanowire array (NA) on the CNTFs substrates [147]. Then, the synthesized CNTFs@$ZnCo_2O_4$ served as $Zn^{2+}$ and $Co^{2+}$ ions source and a skeleton for in situ growth of Zn/Co-ZIF, leading to the formation of core-shell structured $ZnCo_2O_4$ NA@Zn/Co-ZIF. The well-oriented hybrid arrays with a rod-like morphology of $ZnCo_2O_4$ NA@Zn/Co-ZIF possessed a uniform length of several micrometers. After oxidation and sulfurization, CNTFs@$ZnCo_2O_4$@Zn-Co-S hybrid arrays were produced.

Nanotube structure with large surface area and well-defined inner channels could be an ideal support for the in-situ growth of MOFs [148-150]. For example, $MnO_2$ nanotubes with an overall diameter of 85 nm were first prepared by a hydrothermal method and then used as supports for synthesis of 1D hierarchical hollow $MnO_2$@NiCo-LDH/$CoS_2$ hybrids (Fig. 9e) [151]. Relying on the electrostatic interactions, the $MnO_2$ nanotubes with negative charge absorbed $Co^{2+}$ ions onto outer layer and thus formed core–shell structured $MnO_2$@ZIF-67 (Fig. 9f, j and g, k). Upon adding $Ni(NO_3)_2$, the hollow NiCo-LDH nanocages gradually formed on the $MnO_2$ surface by etching reaction, resulting in $MnO_2$@NiCo-LDH precursors (Fig. 9h, l). After sulfuration, the final 1D hollow nanomaterials were obtained (Fig. 9i, m). Remarkably, the $Ni^{2+}$ ions and thioacetamide (TAA) concentration as well as the hydrothermal reaction time were importance to the structure and property of $MnO_2$@NiCo-LDH/$CoS_2$. Based on the similar synthetic route, hierarchical structured bimetallic $Co_3O_4$@$Ni_2P$-CoP/NF hybrids [152] and ternary $CoO/Co_3O_4/CoMoO_4$ composites [153] were fabricated by using $Co_3O_4$ nanowire array and $CoMoO_4$ nanorods as supports, respectively.

Extraneous substrates containing metal compositions combined with MOFs can effectively construct polymetallic hybrids. Each component possesses a special function that can conquer the defects of the individual counterparts and plays unique role in the composites, thus generating a powerful synergistic effect for enhanced performance. In many cases, the integrated substrates not only serve as secondary metal source but also self-sacrificing templates for oriented-growth of morphology. However, this strategy involved pre-design steps is a time-consuming process and may increase the production cost. In situ growth for MOFs and foreign species by one-step method is more expected.

## 4. Electrocatalytic applications

The growing energy demand prompts the exploration and development of efficient materials for chemical energy conversion process. Owing to the rational design and unique properties, MOF-derived multi-metal nanomaterials have been highlighted as electrocatalysts for energy-conversion reactions [154-156]. Besides, MOF-derived electrocatalysts with well-designed structure also can exhibit bi- or tri-functional features, endowing them promising potential in next-generation energy devices such as rechargeable metal-air batteries and overall water splitting. Specifically, electrochemical water splitting involves two half reactions: HER on the cathode electrode and OER on the anode. Besides, ORR is crucial in full cell and metal–air batteries [157]. In this section, the application of MOF-derived multi-metal nanomaterials as catalysts in energy-conversion electrochemical reactions are discussed, including the oxygen reduction reaction, oxygen evolution reaction and hydrogen evolution reaction. The catalytic performances of MOF-derived multi-metallic nanomaterials for electrocatalytic applications have been summarized in Table 2.

### 4.1. ORR

Enormous efforts have been devoted to develop ORR catalysts, which can exhibit high current density at low overpotential. The ORR process proceeds through multiple steps of oxygen-containing intermediates adsorbed on catalyst surface, like associative, dissociative, or peroxospecies formation [158, 159]. Several two-electron and four-electron reactions control the overall efficiency of the catalytic systems. Selective two-electron reduction produces $H_2O_2$ whereas four-electron reduction leads to the formation of $H_2O$. In most cases, the four-electron route is more preferred owing to the superior efficiency. As is well-known, noble metal Pt is recognized as the benchmark electrocatalyst for this process. However, the high cost and the natural scarcity of Pt still hamper its large-scale implementation. Dealloying of Pt with transition metal to expose increased active sites and concurrently reduce the usage of Pt is an effective approach to ensure the superior ORR activity. For example, Chen et al. utilized ZIF-67 as precursor to develop PtCo bimetallic nanoparticles anchored in N-doped carbon capsules PtCo/Co@NHPCC [128]. $H_2PtCl_6 \cdot 6H_2O$ acted as guest molecules were introduced into the pores of Co-based MOFs. Followed by hydrogen reduction and pyrolysis process, the final PtCo/Co@NHPCC was produced. The as-synthesized catalysts showed an excellent ORR performance, with a mass activity that was 5.5 and 13.5 times higher than that of commercial Pt/C and Pt black, respectively. Besides, it was exciting to find that PtCo/Co@NHPCC catalyst achieved a considerably improved durability in terms of both electrochemically active surface area and mass activity, in comparison with commercial Pt/C and Pt black catalysts. The structural features (such as alloy structure, good dispersivity and fine particle size) as well as the carbon matrix are responsible for the outstanding electrocatalytic activity.

Downsizing the noble metal particles to expose more available atoms on the surface is another approach to make Pt-based catalysts more affordable. Atomically dispersed metal catalysts with high atom efficiency have sparked new interest in electrocatalysis [160-162]. In the research of Yao, a locally distributed atomic Pt-Co nitrogen−carbon-based catalyst (A-CoPt-NC) was reported [163]. The obtained catalyst only contained a small content of Co (~1.72 wt %) and a very little Pt (~0.16 wt %). Unexpectedly, it displayed extremely high activities for ORR in alkaline media, delivering mass activity 267 times greater than that of the commercial Pt/C catalyst. No noticeable decay in activity was observed after a 240 min electrochemical durability test. Furthermore, the A-CoPt-NC showed a high selectivity for the 4-electron pathway in ORR, which can be ascribed to the atomic interaction of Pt−Co.

Considering the agglomeration and degradation of Pt-based catalyst during annealing and cycling tests, constructing core-shell structure by combing noble metal and transition metal is highly desirable, because it can increase the catalytic efficiency and simultaneously maintain the structural stability. As an example, a quasi-Pt-allotrope catalyst, comprising of hollow $Pt_3Co$ core and N-doped carbon embedding single-atom Pt shell (H-PtCo@$Pt_1$N-C) was prepared (Fig. 10a) [164]. When tested in

0.1 M $HClO_4$ solution, the mass activity of H-PtCo@Pt1N-C was 1.2 mA $\mu g_{Pt}^{-1}$ at 0.9 V, corresponding to 8, 10 and 3.4 times greater than those of Pt/C (0.15 mA $\mu g_{Pt}^{-1}$), Pt/NPC (0.12 mA $\mu g_{Pt}^{-1}$) and PtCo/NPC (0.35 mA $\mu g_{Pt}^{-1}$), respectively (Fig. 10b). After 10000 cycle tests, the catalyst presented stable activity without any fade, showing the excellent durability towards ORR (Fig. 10c). Benefiting from the synergistic effect between the single Pt atom/N-doped carbon shell and hollow PtCo alloy core, the H-PtCo@$Pt_1$N-C exhibited efficient and stable ORR activities in various organic electrolytes, suggesting its huge potential in next-generation lithium–air batteries.

Owing to the inherent defects of noble metals in reserve and cost, searching for earth-abundant transition metal alternatives with favorable activity and durability is an attractive task for scientific community. In the research of Hassan, C/$NiCo_2O_4$ nanocomposite fibers were constructed by electrospinning method followed by a simple sintering process and utilized as ORR electrocatalyst [165]. The bimetal oxides with mixed valence provided numerous accessible active sites. The half-wave potential of 0.53 V and the initial potential of 0.59 V for C/$NiCo_2O_4$ were more positive than single $NiCo_2O_4$ and carbon free $NiCo_2O_4$. The incorporated carbon can greatly promote the electron transfer, thus imposing a prominent contribution to the electrocatalytic activity. Meng et al. reported a hierarchically structured porous Co-Zn-N-C electrocatalyst for ORR by using ZnCo-ZIF as precursors [166]. The as-prepared HC-5Co95Zn catalysts exhibited excellent half-wave potential (0.78 V vs.

RHE) and diffusion limiting current density (5.7 mA cm$^{-2}$), which were close to those of commercial Pt/C catalyst in acidic solution (Fig. 10d). Besides, the resulted HC-5Co95Zn presented a lower Tafel slope of 66 mV dec$^{-1}$ and better long-term stability compared with that of Pt/C of 75 mV dec$^{-1}$. After 30,000 s stability test, the normalized current of HC-5Co95Zn decreased 12.6%, while Pt/C faded by 36.1% after 20,000 s chronoamperometric response (Fig. 10e). The hierarchical porous architecture was responsible for the remarkable ORR catalytic activity. Wang and co-workers developed hierarchical porous N,S-codoped carbon immobilized with Co-Ni-sulphide nanoparticles (Ni-Co-S@G/NSC) from $NH_2$-MIL-101(Al) [167]. Benefiting from the distinctive nanoarchitectures and the synergetic effect between the active metal species, the Ni-Co-S@G/NSC delivered an ultrahigh power density of 261.3 mW cm$^{-2}$ and high specific capacity density of 2947 mA h g$^{-1}$, as well as comparable onset potential (0.94 V vs. RHE) and half-wave potential (0.86 V vs. RHE) to the commercial Pt/C catalyst in ORR.

### 4.2. OER

As the reverse reaction to the ORR, the OER is vital to many energy-conversion devices as well. Similar to ORR, OER is a complicated four-electron process containing multistep elementary reactions, where $O_2$ generation with different reaction mechanism under acidic and alkaline conditions. Actually, OER normally occurs as a rate determining step due to the intrinsically sluggish kinetics stemming from multistep proton-coupled four-electron transfer process related to the H–O fracture and O–O bonding [168, 169]. At present, noble-metal-based catalysts (e.g., Ir, $IrO_2$, and $RuO_2$) are considered as the benchmark electrocatalysts towards OER. Utilizing MOF-derived multi-metal nanomaterials to replace precious metal catalysts for OER have been widely reported. Owing to the high activity and low cost, transition-metal-oxides has recently attracted significant attention. As an example, 3D $Ni_xCo_{3-x}O_{4-y}$ nanocages were synthesized using Ni-doped ZIF-67 as precursors and investigated their electrocatalytic OER characteristics [170]. Substitution of Ni into $Co_3O_4$ structure helped to improve the inherent catalytic activity. By virtue of the presence of nonstoichiometry and low coordination metal sites, which could reduce the $OH^-$ adsorption energy and promote the conductivity of catalyst, the $Ni_xCo_{3-x}O_{4-y}$ showed enhanced OER activity. The resulting NiCo-1 (Ni/Co = 1) exhibited a lower overpotential of 320 mV at a current density of 10 mA $cm^{-2}$ and a lower Tafel slope of 53 mV $dec^{-1}$. The porous structure and rich redox centers were contributed to the excellent OER performance and made it a competitive electrocatalyst for water oxidation reaction.

Similarly, Ni–Co mixed oxide cages derived from Ni–Co PBA cages were developed as electrocatalysts for OER [48]. The as-prepared catalysts displayed an outstanding performance towards OER with a small overpotential of 0.38 V at the current density of 10 mA $cm^{-2}$. Besides, the catalytic activity of Ni–Co mixed oxide cages was no obvious loss after 10 h of the electrochemical reactions in alkaline medium, showing its good durability. In addition to transition metal oxides, transition metal sulfides also showed their improved catalytic activity for OER [171, 172]. Recently, ultrathin $Co_8FeS_8$/CoS nanoparticles grown on carbon nanotubes (CNTs) skeleton ($Co_8FeS_8$/CoS@CNT) were developed as OER catalyst, which delivered a low overpotential of 278 mV for 10 mA $cm^{-2}$, a very small Tafel slope of 49 mV $dec^{-1}$ as well as good long-run stability [173]. The excellent activity was attributed to the introduction of highly conductive CNTs and the homogenously distributed $Co_8FeS_8$/CoS nanoparticles.

Aside from multi-metal oxides and sulfides, transition-metal-based phosphides also possessed promising potential for OER due to their free noble metal, favorable activity and hydrogenaselike catalytic mechanism. Among them, Co based bimetallic phosphides have been proved as cost-effective OER electrocatalysts. Li et al. fabricated carbon incorporated homobimetallic (CoNi/C, CoCu/C, CoMn/C) phosphide electrocatalyst for OER [174]. The as-obtained CoNi/C-HHPNC showed highest OER activity with a current density of 10 mA $cm^{-2}$ at overpotentials of about 267 mV, much lower than that of the $RuO_2$ (366 mV) [175] and $IrO_2$ (338 mV) [176]. CoMnP/C and CoCuP/C-HHPNC also delivered lower potentials of 262 and 283 mV respectively to reach a current density of 10 mA $cm^{-2}$. In addition, CoNi/C-HHPNC retained 98.6% of the initial current density after 12 h at the overpotential of 280 mV, indicating its long-term stability in regard to the intrinsic functionality. The density functional theory (DFT) calculations demonstrated that the homogenously introduced secondary metals and the incorporated carbon effectively regulated the electronic structure, thus collaboratively resulting in the low kinetic energy barrier for the OER. Using bimetal CoFe-PBA as platform, bimetal cobalt−iron phosphides ($Co_{1-x}Fe_xP$) with uniform metal distribution were achieved [177]. By continuously optimizing the Co/Fe ratio, the best catalytic activity was observed at the Co/Fe ratio of 1.63, which exhibited a small overpotentials of 230 and 268 mV at 10 and 100 mA $cm^{-2}$, respectively, exceeding most of the reported transition-metal phosphides. The superior OER activity could ascribed to the more exposed active sites caused by small size of $Co_{1-x}Fe_xP$ and the electronic modulation due to the Fe doping. Lou et al. fabricated carbon incorporated Ni–Co mixed metal phosphide nanoboxes (NiCoP/C) by two-step methods [178]. Specifically, ZIF-67 nanocubes were synthesized and then reacted with $Ni(NO_3)_2$ to form ZIF-67@Ni–Co layered double hydroxide (LDH) nanoboxes. After phosphidation with $NaH_2PO_2$, the nanocomposite NiCoP/C nanoboxes were produced. Benefiting from the structural and compositional merits, the as-prepared catalysts showed enhanced electrochemical performance and long-term stability for OER, which required an overpotential of 330 mV to attain a current density of 10 mA $cm^{-2}$.

### 4.3. HER

Hydrogen production through electrochemical process is the vital part of clean energy conversion in water splitting and hydrogen fuel cells. The HER pathway involving $H_2$ production contains several steps reactions with two possible mechanisms, which proceed through either the Volmer–Tafel mechanism ($H^+ + e^- \rightarrow H^*$; $2H^* \rightarrow H_2 + 2^*$)

or the Volmer–Heyrovsky mechanism ($H^+ + e^- \rightarrow H^*$; $H^* + H^+ + e^- \rightarrow H_2 + *$) [179]. Unlike ORR and OER reactions, where the O atoms in the intermediates are adsorbed on the catalyst surface, hydrogen intermediates (H*) are adsorbed on the active sites during HER process. Consequently, the hydrogen adsorption energy is a key factor for the selection of electrocatalysts for HER. Developing efficient HER electrocatalysts is essential for sustainable development of a hydrogen-based society. As discussed above, transition-metal-based nanomaterials are regarded as excellent alternatives to precious metal catalysts owing to their intrinsic properties. $MoS_2$ as one of the most intriguing layered materials has been proved to be a promising electrocatalyst for HER [180, 181]. The HER activity of $MoS_2$ has been demonstrated to stem from the edges instead of their basal planes [182]. In the research of Lou, nickel and cobalt incorporated $MoS_2$ nanoboxes derived from Ni–Co PBA were constructed by an ion-exchange process with ammonium thiomolybdate [183]. As a HER catalyst, Ni–Co–$MoS_2$ nanobox manifested the enhanced activity with an onset potential of 125 mV and a small Tafel slope of 51 mV dec$^{-1}$, better than those of 168 mV and 60 mV dec$^{-1}$ for bare $MoS_2$ respectively. The stability of catalysts also was assessed and only negligible decay was observed after 1000 cycles, suggesting the good durability of the resulting Ni–Co–$MoS_2$ nanoboxes for HER. The strong synergism between various metal sulfide phases (i.e., $NiS_x$, $CoS_x$, NiMoS, and CoMoS) and $MoS_2$ may be responsible for the improved HER performance. Similarly, hollow $Co_3S_4$@$MoS_2$ heterostructures were fabricated through two-step temperature-raising hydrothermal process using ZIF-67 as precursors [184]. Core−shell $Co_3S_4$@$MoS_2$ heterostructure was composed of a hollow $Co_3S_4$ polyhedron as the core and $MoS_2$ as the shell. The obtained catalysts showed enhanced HER performance in terms of low overpotential (210 mV at 10 $mA \cdot cm^{-2}$), high current density, and good durability, outperforming to those of individual hollow $Co_3S_4$ polyhedrons and $MoS_2$ nanosheets.

Transition-metal-based nitrides have drawn intense attention recently because the introduced N atoms with negatively charge can modify the d-band density of the parent metals, making the electronic structures of metal nitrides similar to group VIII noble metals [185-187]. Guo et al. prepared porous rodlike cobalt−nickel bimetal nitrides ($Co_xNi_yN$) by nitridation from MOF-74 [188]. Tanks to the structural advantages, uniformed metal dispersion and electron modulation effect. The resulting catalysts exhibited a superior catalytic ability for HER at all pH values. The optimized $Co_2Ni_1N$ delivered overpotentials of 92.0 mV and 102.6 mV at a current density of 10 mA $cm^{-2}$ in acidic and alkaline media, respectively. Furthermore, the $Co_2Ni_1N$ presented ignorable loss of current density after 24 h test, indicating its excellent electrochemical stability in acidic environment. Recently, trimetallic Fe/Co/Cu-based phosphides decorated with N-doped carbon-graphene (FeCoCuP@NC) were fabricated through a facile two-step approach [189]. When used as HER electrocatalyst, FeCoCuP@NC showed superior catalytic performance with low overpotential of 80 and 169 mV at a current density of 10 mA $cm^{-2}$ and low Tafel slopes of 47.6 and 48.8 mV $dec^{-1}$ in 0.5 M $H_2SO_4$ and 1.0 M KOH, respectively.

These values were better than those of FeCoCu@NC without phosphorization, illustrating the positive effect of phosphorization on the HER performance. Besides, the N-doped carbon-graphene matrix, the formation of heterojunctions between different phosphides as well as the cooperation effect between active phosphides were beneficial to the improved HER activity.

### 4.4. Bi-/tri-functional electrocatalysts

In fact, the practical electrochemical devices usually involve more than one process. For example, the metal–air batteries are composed of OER and ORR, and the overall water splitting is related to HER and OER. Considering that, developing multifunctional electrocatalysts performed well in HER, OER and ORR and possess excellent durability is favorable. Multi-metallic nanomaterials derived from MOFs with particular property can provide synergy and are expected to replace precious metals to meet the demand of further development. As an example, Zhao et al. reported a facile synthesis strategy for bimetal phosphide nanotubes for overall water splitting [190]. By adjusting the molar ratio of Co/Ni atoms in MOF-74 precursor, a series of $Co_xNi_yP$ electrocatalysts were fabricated through low-temperature phosphorization. Among them, the as-prepared $Co_4Ni_1P$ with similar morphology to precursor possessed a rare form of nanotubes, and exhibited favorable dispersal of the active sites. The catalysts presented a current density of 10 mA $cm^{-2}$ at overpotentials of 129 mV for HER and 245 mV for OER, respectively. Notably, an electrolyzer using $Co_4Ni_1P$ as both the anode and cathode catalyst in alkaline medium afforded a current density of 10 mA $cm^{-2}$ at a voltage of 1.59 V, which could compete with the Pt/C and $RuO_2$ counterparts. Moreover, $Co_4Ni_1P$ catalysts showed long-term stability with no obvious loss of after 50 h continuous operation.

In another case, the ultrafine and monodispersed NiCoZnP nanoclusters distributed on the ultrathin NC nanosheets (NiCoZnP/NC) were successfully fabricated as binder-free catalysts for overall water splitting [191]. Owing to the small size of NiCoZnP and the hierarchical nanoarchitectures of NC, the catalysts showed large surface area and abundant active sites, thus leading to the enhanced electrocatalytic properties. The self-supported NiCoZnP/NC nanosheets displayed high activity for HER with low overpotential of 74 mV and OER with overpotential of 228 mV at current density of 10 mA $cm^{-2}$ in 1.0 M KOH solution. Also, a low potential of 1.54 V to reach 10 mA $cm^{-2}$ and excellent durability with a little deactivation during 85 h of continuous electrolysis testing were achieved by NiCoZnP/NC.

Designing non-precious electrocatalysts with unique heterostructures is important to improve the electrocatalytic activity. For example, N-doped carbon-decorated CoP@FeCoP yolk-shelled micro-polyhedrons were prepared by phosphorization from ZIF-67@Co-Fe-PBAs (Fig. 11a) [192]. Benefiting from the yolk-shell construction and N-doped carbon matrix, the aggregation degree of CoP was large mitigated, thus leading to the high specific surface area and more exposed active sites. Besides, the synergistic effect between the yolk-shell structure and N-doped carbon also helped to optimize the electronic structure. To drive the current density of 10 mA cm$^{-2}$, the overpotentials of CoP@FeCoP only required 141 and 238 mV in alkaline electrolyte for HER and OER, respectively, lower than those of CoP/NC, ZIF-67 micro-polyhedrons and ZIF-67@Co-Fe PBA (Fig. 11b and c). When used as a two-electrode for water splitting, it needed a low cell voltage of 1.68 V to achieve a current density of 10 mA cm$^{-2}$, much better than that of $RuO_2$||Pt/C electrolyzer, and exhibited good long-term stability after 20 h (Fig. 11d and e). Recently, a unique core–shell structure of $CoSe_2$ laminated with $MoSe_2$ derived from Co-MOF (MOF-$CoSe_2$@$MoSe_2$) was successfully fabricated [193]. MOF-$CoSe_2$@$MoSe_2$ core–shell structure was directly grown on a flexible CC substrate and avoided the usage of binder. The as-prepared core-shell structured CC/MOF-$CoSe_2$@$MoSe_2$ demonstrated a low overpotentials of 109.87 and 183.81 mV for the HER and OER in alkaline media, respectively, and a low voltage of 1.53 V for a two-electrode water electrolysis, outperformed those of CC/MOF and CC/$MoSe_2$.

As for bifunctional oxygen electrocatalysts, Chen et al. reported amorphous bimetallic $Fe_{0.5}Co_{0.5}O_x$ nanoparticles embedded in N-doped reduced graphene oxide (rGO) by using Fe-Co PBAs as precursors [194]. The as-obtained amorphous $Fe_{0.5}Co_{0.5}O_x$ showed superior OER activity with an overpotential of 257 mV for 10 mA cm$^{-2}$ and a Tafel slope of 30.1 mV dec$^{-1}$, as well as excellent ORR activity with a large limiting current density of $-5.25$ mA cm$^{-2}$ at 0.6 V. More importantly, a Zn-air battery delivered a peak power density of 86 mW cm$^{-2}$, a specific capacity of 756 mA h $g_{Zn}^{-1}$ (corresponding to an energy density of 904 W h $kg_{Zn}^{-1}$) and good long-term stability over 120 h at 10 mA $cm^{-2}$. Using the bamboo-like nanofibers composites of Ni–Co-BTC mixed with polyacrylonitrile as precursors, NiCo-0.8@N-CNFs-800 were developed as bifunctional catalysts for ORR and OER [195]. Owing to a highly doped-N content, uniform dispersion of NiCo alloy and decentralized NiCo–$N_x$ active sites, the NiCo-0.8@N-CNFs-800 performed an excellent electrocatalytic performance. Specially, the ORR onset potential on NiCo-0.8@N-CNFs-800 was 0.91 V and the half-wave potential was 0.82 V. Under the OER condition, NiCo-0.8@N-CNFs-800 achieved a minimum potential of 1.61 V at the current density of 10 mA $cm^{-2}$. In recent, atomically isolated binary Co-Ni sites anchored on N-doped hollow CNTs (CoNi-SAs/NC) were constructed by pyrolysis of dopamine-coated CoNi-MOF [196]. By virtue of the rich single-atom active sites and cooperation effect between diatomic structure in porous conductive carbon matrix, the as-synthesized CoNi-SAs/NC showed superior catalytic activity for ORR and OER by presenting low overpotential, high electron transfer number and excellent reversibility in alkaline electrolyte, outperforming many non-precious catalysts. In comparison with single monometallic Ni-N and CoNi counterparts, DFT calculations revealed that the accessibility of atomically dispersed Co-Ni sites and the synergy of dual metal-N structure (Co-Ni-N) were conducing to reducing the energetic barrier and boosting reaction kinetics.

Aside from bifunctional electrocatalysts, the cost-efficient and durable trifunctional heterostructure electrocatalysts for HER, OER and ORR are crucial to overall water splitting and regenerative metal-air batteries. In the research of Yuan, binary FeNi phosphide coupled with N, P-modified carbon nanosheets (FeNiP/NPCS) were synthesized through carbonization-phosphorization method [197]. The structural advantages and optimized electronic structure of FeNiP/NPCS were responsible for the exceptional activity of overall water splitting and rechargeable Zn-air batteries, achieving excellent performance in these energy conversion and storage devices. In another case, $Mo_2C$ nanosheets vertically aligned on the Co-decorated N-doped carbon polyhedron ($Mo_2C$/Co@NC) were successfully constructed [198]. Benefiting from the powerful interfacial effect from $Mo_2C$ nanosheets and Co@NC polyhedron as well as the reciprocally permeated structure, the intrinsic properties and accessible active sites were greatly improved, resulting in high electrocatalytic performance and good durability for HER, OER and ORR (Fig. 12a-f). Using $Mo_2C$/Co@NC as the electrodes, $Mo_2C$/Co@NC-based Zn-air battery could efficiently motivate the electrochemical water splitting. Recently, Lee et al. CoP-N-doped carbon@NiFeP nanoflakes (CoP-NC@NFP) were developed as multifunctional catalysts for water splitting and zinc-air battery [199]. The abundant active catalytic sites in CoP-NC@NFP were contributed to the excellent charge-transfer kinetics and electrocatalytic activity, with an overpotential of 270 and 162 mV for OER and HER, respectively, and a Tafel slope of 46 mV dec$^{-1}$ for ORR (Fig. 12g). With respective to overall water splitting device, CoP-NC@NFP required a cell voltage of 1.57 V to attain a current density of 10 mA cm$^{-2}$ (Fig. 12h). Besides, zinc-air batteries assembled with CoP-NC@NFP as the air–cathode presented high power density of 93 mW cm$^{-2}$ (Fig. 12i). These multifunctional electrocatalysts free of noble metals with remarkable activity and excellent stability opens a practical possibility for clean energy production and storage.

Optimizing the performance of electrocatalysts requires atomic-scale investigation yet it still remains grand challenges for all scientists. To gain an in-depth understanding for the catalytic behavior of multi-metallic nanomaterials in electrocatalysis, the precise identification of catalytically active sites is highly necessary because it can reveal the interaction mechanism between metal species. Active sites of electrocatalysts and their catalytic properties can be experimentally demonstrated, the direct observation of intermediates in reaction process is also important for indisputable results. Recently, using in situ characterization approaches is helpful for probing catalyst states and important reaction intermediates on electrochemical conditions. Specifically, vibrational spectroscopic technologies, including Raman and Fourier transform infrared spectroscopy (FTIR)-based methods, are proved to be effective tools to identify active sites, surface state changes, and interfacial intermediates under operando conditions [200]. Noteworthy, Raman or FTIR alone is unable to provide a comprehensive information of a complex catalytic system. Raman is better than FTIR in probing bond vibrations in low frequency range without water interference. While FTIR has an edge over in confirming the role of interfacial water and adsorbed electrolytes.

Furthermore, other in situ characterization approaches, such as in situ X-ray photoelectron spectroscopy (XPS) and in situ X-ray absorption spectroscopy (XAS), differential electrochemical mass spectrometry (DEMS), and Mössbauer spectroscopy, also can be employed to attain wide insights into the surface evolution and interfacial reaction occurring in electrocatalytic process [72, 201, 202]. For example, Görlin et al. reported a kinetic study of Ni–Fe LDH on OER conditions [201]. The combined DEMS and XAS analyses verified that the addition of Fe could improve the kinetics of the metal-reduction step, leading to an enhancement of the OER activity. In order to obtain the comprehensive information related to the evolution of the structure, composition and surface state changes of $Co_2FeO_4$ and $CoFe_2O_4$ NPs, many characterization methods including XAS, XPS, atom probe tomography (APT) and high-resolution transmission electron microscopy (HRTEM) were utilized during cyclic voltammetry (CV) measurements under OER conditions [203]. Using in situ attenuated total reflection-based FTIR (ATR-FTIR) spectroscopy, Nayak et al. determined the reaction intermediates of ORR on nanostructured Pt electrodes [204]. Based on XAS analysis, Wang et al. concluded that the NiOOH phase instead of Ni–Co spinel itself served as the main redox sites because only Ni displayed redox behavior for OER process [205]. To gain more direct evidence for understanding the real structure of multi-metal nanomaterials as well as their catalytic mechanisms, more advanced instruments and techniques are highly needed.

## 5. Summary and outlook

The secondary-metal incorporation is confirmed to provide new geometrically active sites for catalysts or manipulate the inherent electronic and/or surface structures by electron transfer between host and guest metals toward a powerful synergetic effect for higher catalytic activity [206, 207]. Because of the different electron-donating abilities of metals, the changes in electronic structure are different, in turn affecting the catalytic properties. Besides, the incorporation of foreign metals can offer additional active sites by activating inert atomic sites, leading to an enhanced catalysis [208]. Based on the adsorption energy calculations, screening of promising metal combinations has been conducted by selecting appropriate dopants. Herein, the superiorities of MOF for construction of multi-metal nanomaterials are summarized. Importantly, six primary design strategies for multi-metallic nanomaterials from MOFs are emphasized. It should be remarked that although these strategies are separately discussed, two or more pathways are adopted simultaneously in some cases. The combination of different synthetic approaches can afford vast opportunities for developing other novel polymetallic materials. Then, the recent advances of MOF-derived multi-metal nanomaterials for electrocatalytic applications (mainly focus on ORR, OER and HER) is comprehensively discussed. These examples reported till now are truly inspiring, and the nanostructured materials with multi-metallic components using MOFs as precursors/templates have an extremely bright future.

Despite the achieved success in the transformation of polymetallic MOFs to their corresponding derivatives, this research field is still at a burgeoning stage, and more endeavor is required to realize the precise synthesis and large-scale production. Several challenges and personal perspective related to future development are critically proposed as follows:

1) The transformation mechanism from MOFs to their derivatives should be deeply explored. As we know, the particle size, shape and stoichiometry greatly affect the activity, selectively and stability of catalysts; however, these parameters are difficult to rationally control during the synthetic process. Thus, more investigations about precise synthesis are highly desirable. Meanwhile, the delicate modulation of geometric structures can be achieved through precise synthesis.

2) The construction of MOF derivatives with multiple metals should be considered. To date, many researchers tend to fabricate bimetallic materials. More efforts should be devoted to introducing three or more metals into a MOF skeleton while retain the integrity of structure. Multi-metal ions with different oxidation states can provide more catalytic sites for the electrochemical reaction, leading to improved intrinsic activity. In addition, the function of metal nodes in catalysis has been widely studied, but the researches on the role of organic ligands are

scarce. Therefore, much attention is required to verify the contribution of each component in multi-metallic materials.

3) Different morphologies and structures for polymetallic nanomaterials should be developed. Currently, examples presented mainly focus on the simple hollow and core-shell structures. It is urgent to design new shapes of MOF-derived multi-metallic nanomaterials with abundant active sites, such as cube-, polyhedron-, sheet-, cylinder-, chestnut- or seaurchin-like ones, enabling them to adapt more challenging reactions under harsh conditions. Meanwhile, the morphology of most materials used for catalysis is nanoparticles, which is easy to self-aggregate, leading to a reduction of the number of active sites. Therefore, more complex nanostructures are eager to enrich the warehouse of MOF-derived multi-metallic nanomaterials, such as 0D quantum dots, 2D nanosheets and single atoms.
4) Advanced characterizations combined with the auxiliary computational calculations are highly recommended. At present, many studies simply attributed the enhanced activity to the synergistic effect; whereas, the real origin of such an effect is still indistinct. To improve the utilization efficiency of these functional materials, it is of critical importance to investigate the specific active centers, the location of second metal and the interactions between different metal components. Therefore, using some advanced technologies such as X-ray absorption spectroscopy comprising both XANES and EXAFS, aberration-corrected HAADF-STEM, and DFT calculations to reveal the real-time structural evolution

and better design experiments is necessary, thus providing theoretical guidance for the preparation of multi-metallic nanomaterials from MOFs with high performance.

5) Novel synthetic protocols for well-designed nanomaterials are imperatively needed. The synthesis of polymetallic MOF derivatives usually involves several calcination steps at high temperature, which is averse to preserve the periodic pore structure from parent MOFs. Moreover, the generated toxic tail gas during pyrolysis might increase the environmental risks. As the practical applications are the ultimate goal, the optimization on synthetic procedure is eager to achieve the mass production and low cost for industrial applications.

In conclusion, the large diversity of MOF structures and compositions makes them as suitable platform for the construction of polymetallic nanomaterials with desirable properties. The rapid development of these functional materials will bring excellent opportunities in the fields such as adsorption, catalysis, energy conversion and storage and so on, much beyond that of monometallic materials derived from MOFs. In the near future, numerous efforts should be devoted to this exciting area to realize the large-scale engineering and commercial applications.

## Acknowledgements

This work was supported by the National Natural Science Foundation of China (No. 51521006, 52070077, 51879101), the National Program for Support of Top–

Notch Young Professionals of China (2014), the Program for Changjiang Scholars and Innovative Research Team in University (IRT-13R17), the Hunan Provincial Science and Technology Plan Project (2018SK20410, 2017SK2243, 2016RS3026), the Fundamental Research Funds for the Central Universities (531118010226), and Hunan Provincial Innovation Foundation For Postgraduate (CX20200415).

## References

[1] Choudhary N, Li C, Moore J, Nagaiah N, Zhai L, Jung Y, Thomas J. Asymmetric supercapacitor electrodes and devices. Adv. Mater. 2017;29:1605336.

[2] Shao Y, El-Kady M F, Sun J, Li Y, Zhang Q, Zhu M, Wang H, Dunn B, Kaner R B. Design and mechanisms of asymmetric supercapacitors. Chem. Rev. 2018;118:9233-9280.

[3] Zhao Q, Song A, Ding S, Qin R, Cui Y, Li S, Pan F. Preintercalation Strategy in Manganese Oxides for Electrochemical Energy Storage: Review and Prospects. Adv. Mater. 2020;2002450.

[4] Yang Y, Li X, Zhou C, Xiong W, Zeng G, Huang D, Zhang C, Wang W, Song B, Tang X. Recent advances in application of graphitic carbon nitride-based catalysts for degrading organic contaminants in water through advanced oxidation processes beyond photocatalysis: A critical review. Water Res. 2020;116200.

[5] Zhou X, Zeng Z, Zeng G, Lai C, Xiao R, Liu S, Huang D, Qin L, Liu X, Li B. Persulfate activation by swine bone char-derived hierarchical porous carbon: Multiple mechanism system for organic pollutant degradation in aqueous media. Chem. Eng. J. 2020;383:123091.

[6] Li X, Zheng S, Jin L, Li Y, Geng P, Xue H, Pang H, Xu Q. Metal‐Organic Framework‐Derived Carbons for Battery Applications. Advanced Energy Materials. 2018;8:1800716.

[7] Cho J, Jeong S, Kim Y. Commercial and research battery technologies for electrical energy storage applications. Prog. Energy Combust. Sci. 2015;48:84-101.

[8] Zhang G, Li Y, Xiao X, Shan Y, Bai Y, Xue H-G, Pang H, Tian Z, Xu Q. In Situ Anchoring Polymetallic Phosphide Nanoparticles within Porous Prussian Blue Analogue Nanocages for Boosting Oxygen Evolution Catalysis. Nano Lett. 2021;21:3016-3025.

[9] Sadhasivam T, Dhanabalan K, Roh S-H, Kim T-H, Park K-W, Jung S, Kurkuri M D, Jung H-Y. A comprehensive review on unitized regenerative fuel cells: Crucial challenges and developments. Int. J. Hydrogen Energy. 2017;42:4415-4433.

[10] Aurbach D, McCloskey B D, Nazar L F, Bruce P G. Advances in understanding mechanisms underpinning lithium–air batteries. Nature Energy. 2016;1:1-11.

[11] Roger I, Shipman M A, Symes M D. Earth-abundant catalysts for electrochemical and photoelectrochemical water splitting. Nature Reviews Chemistry. 2017;1:1-13.

[12] Zheng Y, Jiao Y, Jaroniec M, Qiao S Z. Advancing the electrochemistry of the hydrogen‐evolution reaction through combining experiment and theory. Angew. Chem. Int. Ed. 2015;54:52-65.

[13] Wang H, Chen K, Cao Y, Zhu J, Jiang Y, Feng L, Dai X, Zou G. High-performance oxygen reduction catalyst derived from porous, nitrogen-doped carbon nanosheets. Nanotechnology. 2016;27:405401.

[14] Seitz L C, Dickens C F, Nishio K, Hikita Y, Montoya J, Doyle A, Kirk C, Vojvodic A, Hwang H Y, Norskov J K. A highly active and stable IrOx/SrIrO3 catalyst for the oxygen evolution reaction. Science. 2016;353:1011-1014.

[15] Sui S, Wang X, Zhou X, Su Y, Riffat S, Liu C-j. A comprehensive review of Pt electrocatalysts for the oxygen reduction reaction: Nanostructure, activity, mechanism and carbon support in PEM fuel cells. Journal of Materials Chemistry A. 2017;5:1808-1825.

[16] Diaz-Morales O, Raaijman S, Kortlever R, Kooyman P J, Wezendonk T, Gascon J, Fu W, Koper M T. Iridium-based double perovskites for efficient water oxidation in acid media. Nature communications. 2016;7:1-6.

[17] Jung N, Cho Y-H, Ahn M, Lim J W, Kang Y S, Chung D Y, Kim J, Cho Y-H, Sung Y-E. Methanol-tolerant cathode electrode structure composed of heterogeneous composites to overcome methanol crossover effects for direct methanol fuel cell. Int. J. Hydrogen Energy. 2011;36:15731-15738.

[18] Cheng X, Shi Z, Glass N, Zhang L, Zhang J, Song D, Liu Z-S, Wang H, Shen J. A review of PEM hydrogen fuel cell contamination: Impacts, mechanisms, and mitigation. J. Power Sources. 2007;165:739-756.

[19] Luo Y, Ahmad M, Schug A, Tsotsalas M. Rising Up: Hierarchical Metal-Organic Frameworks in Experiments and Simulations. Adv. Mater. 2019;31.

[20] Raza W, Kukkar D, Saulat H, Raza N, Azam M, Mehmood A, Kim K-H. Metal-organic frameworks as an emerging tool for sensing various targets in aqueous and biological media. Trac-Trends in Analytical Chemistry. 2019;120.

[21] Shi L, Benetti D, Li F, Wei Q, Rosei F. Phase-junction design of MOF-derived TiO2 photoanodes sensitized with quantum dots for efficient hydrogen generation. Applied Catalysis B-Environmental. 2020;263.

[22] Yang X, Cai J, Wang X, Li Y, Wu Z, Wu W D, Chen X D, Sun J, Sun S P, Wang Z. A Bimetallic Fe-Mn Oxide-Activated Oxone for In Situ Chemical Oxidation (ISCO) of Trichloroethylene in Groundwater: Efficiency, Sustained Activity, and Mechanism Investigation. Environ. Sci. Technol. 2020;54:3714-3724.

[23] Li Y, Han W, Wang R, Weng L T, Yeung K L. Performance of an Aliovalent-Substituted CoCeOx Catalyst from Bimetallic MOF for VOC Oxidation in Air. Applied Catalysis B: Environmental. 2020;119121.

[24] Ye Z, Padilla J A, Xuriguera E, Brillas E, Sires I. Magnetic MIL(Fe)-type MOF-derived N-doped nano-ZVI@C rods as heterogeneous catalyst for the electro-Fenton degradation of gemfibrozil in a complex aqueous matrix. Applied Catalysis B-Environmental. 2020;266.

[25] Wang C, Kim J, Tang J, Kim M, Lim H, Malgras V, You J, Xu Q, Li J, Yamauchi Y. New strategies for novel MOF-derived carbon materials based on nanoarchitectures. Chem. 2020;6:19-40.

[26] Li X, Yang X, Xue H, Pang H, Xu Q. Metal–organic frameworks as a platform for clean energy applications. EnergyChem. 2020;2:100027.

[27] Zhou D-D, Zhang X-W, Mo Z-W, Xu Y-Z, Tian X-Y, Li Y, Chen X-M, Zhang J-P. Adsorptive separation of carbon dioxide: from conventional porous materials to metal–organic frameworks. EnergyChem. 2019;1:100016.

[28] Zhang L, Liu H, Shi W, Cheng P. Synthesis strategies and potential applications of metal-organic frameworks for electrode materials for rechargeable lithium ion batteries. Coord. Chem. Rev. 2019;388:293-309.

[29] He Y, Wang Z, Wang H, Wang Z, Zeng G, Xu P, Huang D, Chen M, Song B, Qin H. Metal-organic framework-derived nanomaterials in environment related fields: Fundamentals, properties and applications. Coord. Chem. Rev. 2020;213618.

[30] Geng P, Wang L, Du M, Bai Y, Li W, Liu Y, Chen S, Braunstein P, Xu Q, Pang H. MIL-96-Al for Li-S Batteries: Shape or Size? Adv. Mater. 2022;34:2107836.

[31] Zheng S, Sun Y, Xue H, Braunstein P, Huang W, Pang H. Dual-ligand and hard-soft-acid-base strategies to optimize metal-organic framework nanocrystals for stable electrochemical cycling performance. National Science Review. 2021.

[32] Farrusseng D, Aguado S, Pinel C. Metal–organic frameworks: opportunities for catalysis. Angew. Chem. Int. Ed. 2009;48:7502-7513.

[33] Liu J, Chen L, Cui H, Zhang J, Zhang L, Su C-Y. Applications of metal–organic frameworks in heterogeneous supramolecular catalysis. Chem. Soc. Rev. 2014;43:6011-6061.

[34] Corma A, García H, Llabrés i Xamena F. Engineering metal organic frameworks for heterogeneous catalysis. Chem. Rev. 2010;110:4606-4655.

[35] Zheng S, Li Q, Xue H, Pang H, Xu Q. A highly alkaline-stable metal oxide@metal-organic framework composite for high-performance electrochemical energy storage. National Science Review. 2020;7:305-314.

[36] Wu Y, Li Y, Gao J, Zhang Q. Recent advances in vacancy engineering of metal-organic frameworks and their derivatives for electrocatalysis. SusMat. 2021;1:66-87.

[37] Cao L-M, Lu D, Zhong D-C, Lu T-B. Prussian blue analogues and their derived nanomaterials for electrocatalytic water splitting. Coord. Chem. Rev. 2020;407:213156.

[38] Chen L, Wang H-F, Li C, Xu Q. Bimetallic metal–organic frameworks and their derivatives. Chemical Science. 2020.

[39] Chen Z, Qing H, Zhou K, Sun D, Wu R. Metal-organic framework-derived nanocomposites for electrocatalytic hydrogen evolution reaction. Prog. Mater Sci. 2020;108.

[40] Huang H, Shen K, Chen F, Li Y. Metal–Organic Frameworks as a Good Platform for the Fabrication of Single-Atom Catalysts. ACS Catalysis. 2020;10:6579-6586.

[41] Yang W, Li X, Li Y, Zhu R, Pang H. Applications of Metal-Organic-Framework-Derived Carbon Materials. Adv. Mater. 2019;31.

[42] Hu H, Zhang J, Guan B, Lou X W. Unusual formation of CoSe@ carbon nanoboxes, which have an inhomogeneous shell, for efficient lithium storage. Angew. Chem. Int. Ed. 2016;55:9514-9518.

[43] Yu X-Y, Feng Y, Guan B, Lou X W D, Paik U. Carbon coated porous nickel phosphides nanoplates for highly efficient oxygen evolution reaction. Energy & Environmental Science. 2016;9:1246-1250.

[44] Zhu C, Liu F, Ling C, Jiang H, Wu H, Li A. Growth of graphene-supported hollow cobalt sulfide nanocrystals via MOF-templated ligand exchange as surface-bound radical sinks for highly efficient bisphenol A degradation. Applied Catalysis B: Environmental. 2019;242:238-248.

[45] Chen J, Liu J, Xie J-Q, Ye H, Fu X-Z, Sun R, Wong C-P. Co-Fe-P nanotubes electrocatalysts derived from metal-organic frameworks for efficient hydrogen evolution reaction under wide pH range. Nano Energy. 2019;56:225-233.

[46] Tang C, Wang H S, Wang H F, Zhang Q, Tian G L, Nie J Q, Wei F. Spatially confined hybridization of nanometer‐sized NiFe hydroxides into nitrogen‐doped graphene frameworks leading to superior oxygen evolution reactivity. Adv. Mater. 2015;27:4516-4522.

[47] Nai J, Yin H, You T, Zheng L, Zhang J, Wang P, Jin Z, Tian Y, Liu J, Tang Z. Efficient electrocatalytic water oxidation by using amorphous Ni–Co double hydroxides nanocages. Advanced Energy Materials. 2015;5:1401880.

[48] Han L, Yu X Y, Lou X W. Formation of prussian‐blue‐analog nanocages via a direct etching method and their conversion into ni‐co‐mixed oxide for enhanced oxygen evolution. Adv. Mater. 2016;28:4601-4605.

[49] Yang X, Wang S, Denis Y, Rogach A L. Direct conversion of metal-organic frameworks into selenium/selenide/carbon composites with high sodium storage capacity. Nano Energy. 2019;58:392-398.

[50] Zhou X, Zeng Z, Zeng G, Lai C, Xiao R, Liu S, Huang D, Qin L, Liu X, Li B. Insight into the mechanism of persulfate activated by bone char: Unraveling the role of functional structure of biochar. Chem. Eng. J. 2020;401:126127.

[51] Sun L, Yildiz B. Solubility Limit of Cu and Factors Governing the Reactivity of Cu–CeO2 Assessed from First-Principles Defect Chemistry and Thermodynamics. The Journal of Physical Chemistry C. 2018;123:399-409.

[52] Selima S, Khairy M, Mousa M. Comparative studies on the impact of synthesis methods on structural, optical, magnetic and catalytic properties of CuFe2O4. Ceram. Int. 2019;45:6535-6540.

[53] Song B, Gong J, Tang W, Zeng G, Chen M, Xu P, Shen M, Ye S, Feng H, Zhou C. Influence of multi-walled carbon nanotubes on the microbial biomass, enzyme activity, and bacterial community structure in 2, 4-dichlorophenol-contaminated sediment. Sci. Total Environ. 2020;713:136645.

[54] Li X, Zeng Z, Zeng G, Wang D, Xiao R, Wang Y, Zhou C, Yi H, Ye S, Yang Y. A “bottle-around-ship” like method synthesized yolk-shell Ag3PO4@ MIL-53 (Fe) Z-scheme photocatalysts for enhanced tetracycline removal. J. Colloid Interface Sci. 2020;561:501-511.

[55] Wang Z, Wang H, Wang Z, Huang D, Qin H, He Y, Chen M, Zeng G, Xu P. Ferrocene modified g-C3N4 as a heterogeneous catalyst for photo-assisted activation of persulfate for the degradation of tetracycline. Colloids and Surfaces A: Physicochemical and Engineering Aspects. 2021;626:127024.

[56] Zhao X, Wu W, Jing G, Zhou Z. Activation of sulfite autoxidation with CuFe2O4 prepared by MOF-templated method for abatement of organic contaminants. Environ. Pollut. 2020;260:114038.

[57] Yang S, Qiu X, Jin P, Dzakpasu M, Wang X C, Zhang Q, Yang L, Ding D, Wang W, Wu K. MOF-templated synthesis of CoFe2O4 nanocrystals and its coupling with peroxymonosulfate for degradation of bisphenol A. Chem. Eng. J. 2018;353:329-339.

[58] Krivanek O L, Chisholm M F, Nicolosi V, Pennycook T J, Corbin G J, Dellby N, Murfitt M F, Own C S, Szilagyi Z S, Oxley M P. Atom-by-atom structural and chemical analysis by annular dark-field electron microscopy. Nature. 2010;464:571-574.

[59] Chen W, Han B, Tian C, Liu X, Liang S, Deng H, Lin Z. MOFs-derived ultrathin holey Co3O4 nanosheets for enhanced visible light CO2 reduction. Applied Catalysis B: Environmental. 2019;244:996-1003.

[60] He Y, Hwang S, Cullen D A, Uddin M A, Langhorst L, Li B, Karakalos S, Kropf A J, Wegener E C, Sokolowski J. Highly active atomically dispersed CoN 4 fuel cell cathode catalysts derived from surfactant-assisted MOFs: carbon-shell confinement strategy. Energy & Environmental Science. 2019;12:250-260.

[61] Chen L, Zuo X, Yang S, Cai T, Ding D. Rational design and synthesis of hollow Co3O4@ Fe2O3 core-shell nanostructure for the catalytic degradation of norfloxacin by coupling with peroxymonosulfate. Chem. Eng. J. 2019;359:373-384.

[62] Chen H, Shen K, Chen J, Chen X, Li Y. Hollow-ZIF-templated formation of a ZnO@ C–N–Co core–shell nanostructure for highly efficient pollutant photodegradation. Journal of Materials Chemistry A. 2017;5:9937-9945.

[63] Wang H, Almatrafi E, Wang Z, Yang Y, Xiong T, Yu H, Qin H, Yang H, He Y, Zhou C. Self-Assembly Hybridization of COFs and g-C3N4: Decipher the Charge Transfer Channel for Enhanced Photocatalytic Activity. J. Colloid Interface Sci. 2021;608:1051-1063.

[64] Li X, Bi W, Chen M, Sun Y, Ju H, Yan W, Zhu J, Wu X, Chu W, Wu C. Exclusive Ni–N4 sites realize near-unity CO selectivity for electrochemical CO2 reduction. J. Am. Chem. Soc. 2017;139:14889-14892.

[65] Wang Z, Wang H, Zeng Z, Zeng G, Xu P, Xiao R, Huang D, Chen X, He L, Zhou C, Yang Y, Wang Z, Wang W, Xiong W. Metal-organic frameworks derived $Bi_2O_2CO_3$/porous carbon nitride: A nanosized Z-scheme systems with enhanced photocatalytic activity. Applied Catalysis B-Environmental. 2020;267:118700.

[66] Xu Y, Tu W, Zhang B, Yin S, Huang Y, Kraft M, Xu R. Nickel Nanoparticles Encapsulated in Few‐Layer Nitrogen‐Doped Graphene Derived from Metal‐Organic Frameworks as Efficient Bifunctional Electrocatalysts for Overall Water Splitting. Adv. Mater. 2017;29:1605957.

[67] Fominykh K, Tok G C, Zeller P, Hajiyani H, Miller T, Döblinger M, Pentcheva R, Bein T, Fattakhova‐Rohlfing D. Rock salt Ni/Co oxides with unusual nanoscale‐stabilized composition as water splitting electrocatalysts. Adv. Funct. Mater. 2017;27:1605121.

[68] Lu X-F, Liao P-Q, Wang J-W, Wu J-X, Chen X-W, He C-T, Zhang J-P, Li G-R, Chen X-M. An alkaline-stable, metal hydroxide mimicking metal–organic framework for efficient electrocatalytic oxygen evolution. J. Am. Chem. Soc. 2016;138:8336-8339.

[69] Li W, Guo X, Geng P, Du M, Jing Q, Chen X, Zhang G, Li H, Xu Q, Braunstein P, Pang H. Rational Design and General Synthesis of Multimetallic Metal-Organic Framework Nano-Octahedra for Enhanced Li-S Battery. Adv. Mater. 2021;33:2105163.

[70] Calle-Vallejo F, Koper M T M, Bandarenka A S. Tailoring the catalytic activity of electrodes with monolayer amounts of foreign metals. Chem. Soc. Rev. 2013;42:5210-5230.

[71] Stephens I E L, Bondarenko A S, Perez-Alonso F J, Calle-Vallejo F, Bech L, Johansson T P, Jepsen A K, Frydendal R, Knudsen B P, Rossmeisl J, Chorkendorff I. Tuning the Activity of Pt(111) for Oxygen Electroreduction by Subsurface Alloying. J. Am. Chem. Soc. 2011;133:5485-5491.

[72] Kim J S, Kim B, Kim H, Kang K. Recent Progress on Multimetal Oxide Catalysts for the Oxygen Evolution Reaction. Advanced Energy Materials. 2018;8.

[73] . lvarez A, Bansode A, Urakawa A, Bavykina A V, Wezendonk T A, Makkee M, Gascon J, Kapteijn F. Challenges in the greener production of formates/formic acid, methanol, and DME by heterogeneously catalyzed CO2 hydrogenation processes. Chem. Rev. 2017;117:9804-9838.

[74] Kasatkin I, Kurr P, Kniep B, Trunschke A, Schlögl R. Role of lattice strain and defects in copper particles on the activity of Cu/ZnO/Al2O3 catalysts for methanol synthesis. Angew. Chem. Int. Ed. 2007;46:7324-7327.

[75] Zhang Q, Xiao Y, Li Y, Zhao K, Deng H, Lou Y, Chen J, Cheng L. NiS‐Decorated ZnO/ZnS Nanorod Heterostructures for Enhanced Photocatalytic Hydrogen Production: Insight into the Role of NiS. Solar RRL. 2020;4:1900368.

[76] Zhang H, Hwang S, Wang M, Feng Z, Karakalos S, Luo L, Qiao Z, Xie X, Wang C, Su D, Shao Y, Wu G. Single Atomic Iron Catalysts for Oxygen Reduction in Acidic Media: Particle Size Control and Thermal Activation. J. Am. Chem. Soc. 2017;139:14143-14149.

[77] Xia W, Zhu J, Guo W, An L, Xia D, Zou R. Well-defined carbon polyhedrons prepared from nano metal-organic frameworks for oxygen reduction. Journal of Materials Chemistry A. 2014;2:11606-11613.

[78] Chen Y-Z, Wang C, Wu Z-Y, Xiong Y, Xu Q, Yu S-H, Jiang H-L. From Bimetallic Metal-Organic Framework to Porous Carbon: High Surface Area and Multicomponent Active Dopants for Excellent Electrocatalysis. Adv. Mater. 2015;27:5010-5016.

[79] Lee K J, Lee J H, Jeoung S, Moone H R. Transformation of Metal-Organic Frameworks/Coordination Polymers into Functional Nanostructured Materials: Experimental Approaches Based on Mechanistic Insights. Acc. Chem. Res. 2017;50:2684-2692.

[80] Lu J, Zhou W, Wang L, Jia J, Ke Y, Yang L, Zhou K, Liu X, Tang Z, Li L, Chen S. Core-Shell Nanocomposites Based on Gold Nanoparticle@Zinc-Iron-Embedded Porous Carbons Derived from Metal-Organic Frameworks as Efficient Dual Catalysts for Oxygen Reduction and Hydrogen Evolution Reactions. Acs Catalysis. 2016;6:1045-1053.

[81] Su H, Wang H-H, Zhang B, Wang K-X, Li X-H, Chen J-S. Enriching Co nanoparticles inside carbon nanofibers via nanoscale assembly of metal-organic complexes for highly efficient hydrogen evolution. Nano Energy. 2016;22:79-86.

[82] Long J, Shen K, Li Y. Bifunctional N-Doped Co@C Catalysts for Base-Free Transfer Hydrogenations of Nitriles: Controllable Selectivity to Primary Amines vs Imines. Acs Catalysis. 2017;7:275-284.

[83] Xu G, Ding B, Shen L, Nie P, Han J, Zhang X. Sulfur embedded in metal organic framework-derived hierarchically porous carbon nanoplates for high performance lithium-sulfur battery. Journal of Materials Chemistry A. 2013;1:4490-4496.

[84] Cao F, Zhao M, Yu Y, Chen B, Huang Y, Yang J, Cao X, Lu Q, Zhang X, Zhang Z, Tan C, Zhang H. Synthesis of Two-Dimensional CoS1.097/Nitrogen-Doped Carbon Nanocomposites Using Metal-Organic Framework Nanosheets as Precursors for Supercapacitor Application. J. Am. Chem. Soc. 2016;138:6924-6927.

[85] Guan C, Liu X, Ren W, Li X, Cheng C, Wang J. Rational Design of Metal-Organic Framework Derived Hollow NiCo2O4 Arrays for Flexible Supercapacitor and Electrocatalysis. Advanced Energy Materials. 2017;7.

[86] Xia W, Zou R, An L, Xia D, Guo S. A metal-organic framework route to in situ encapsulation of Co@Co3O4@C core@bishell nanoparticles into a highly ordered porous carbon matrix for oxygen reduction. Energy & Environmental Science. 2015;8:568-576.

[87] Li X, Wang X, Zhou J, Han L, Sun C, Wang Q, Su Z. Ternary hybrids as efficient bifunctional electrocatalysts derived from bimetallic metal–organic-frameworks for overall water splitting. Journal of Materials Chemistry A. 2018;6:5789-5796.

[88] Wu L L, Wang Z, Long Y, Li J, Liu Y, Wang Q S, Wang X, Song S Y, Liu X, Zhang H J. Multishelled NixCo3 ‐ xO4 Hollow Microspheres Derived from Bimetal ‐ Organic Frameworks as Anode Materials for High ‐ Performance Lithium ‐ Ion Batteries. Small. 2017;13:1604270.

[89] Torad N L, Hu M, Kamachi Y, Takai K, Imura M, Naito M, Yamauchi Y. Facile synthesis of nanoporous carbons with controlled particle sizes by direct carbonization of monodispersed ZIF-8 crystals. Chem. Commun. 2013;49:2521-2523.

[90] Gao J, Cong J, Wu Y, Sun L, Yao J, Chen B. Bimetallic Hofmann-type metal–organic framework nanoparticles for efficient electrocatalysis of oxygen evolution reaction. ACS Applied Energy Materials. 2018;1:5140-5144.

[91] Hu P, Zhuang J, Chou L-Y, Lee H K, Ling X Y, Chuang Y-C, Tsung C-K. Surfactant-directed atomic to mesoscale alignment: Metal nanocrystals encased individually in single-crystalline porous nanostructures. J. Am. Chem. Soc. 2014;136:10561-10564.

[92] Lu G, Li S, Guo Z, Farha O K, Hauser B G, Qi X, Wang Y, Wang X, Han S, Liu X. Imparting functionality to a metal–organic framework material by controlled nanoparticle encapsulation. Nature chemistry. 2012;4:310-316.

[93] Jiang H, Yan Q, Chen R, Xing W. Synthesis of Pd@ ZIF-8 via an assembly method: Influence of the molar ratios of Pd/Zn2+ and 2-methylimidazole/Zn2+. Microporous Mesoporous Mater. 2016;225:33-40.

[94] Dhakshinamoorthy A, Asiri A M, Garcia H. Metal organic frameworks as versatile hosts of Au nanoparticles in heterogeneous catalysis. Acs Catalysis. 2017;7:2896-2919.

[95] Han Y, Xu H, Su Y, Xu Z-L, Wang K, Wang W. Noble metal (Pt, Au@ Pd) nanoparticles supported on metal organic framework (MOF-74) nanoshuttles as high-selectivity CO2 conversion catalysts. J. Catal. 2019;370:70-78.

[96] Pan Y, Heryadi D, Zhou F, Zhao L, Lestari G, Su H, Lai Z. Tuning the crystal morphology and size of zeolitic imidazolate framework-8 in aqueous solution by surfactants. CrystEngComm. 2011;13:6937-6940.

[97] Zhan G, Zeng H C. A Synthetic Protocol for Preparation of Binary Multi-shelled Hollow Spheres and Their Enhanced Oxidation Application. Chem. Mater. 2017;29:10104-10112.

[98] Wang X, Zhang H, Lin H, Gupta S, Wang C, Tao Z, Fu H, Wang T, Zheng J, Wu G. Directly converting Fe-doped metal–organic frameworks into highly active and stable Fe-NC catalysts for oxygen reduction in acid. Nano Energy. 2016;25:110-119.

[99] Tao Z, Wang T, Wang X, Zheng J, Li X. MOF-Derived Noble Metal Free Catalysts for Electrochemical Water Splitting. Acs Applied Materials & Interfaces. 2016;8:35390-35397.

[100] Wang, Zhihao, Jin, Huihui, Meng, Tian, Liao, Ke, Wenqian, Yang. Fe, Cu-Coordinated ZIF-Derived Carbon Framework for Efficient Oxygen Reduction Reaction and Zinc-Air Batteries. Adv. Funct. Mater. 2018;28:1802596.

[101] Zhang K, Zhang Y, Zhang Q, Liang Z, Gu L, Guo W, Zhu B, Guo S, Zou R. Metal ‐ organic framework ‐ derived Fe/Cu ‐ substituted Co nanoparticles embedded in CNTs ‐ grafted carbon polyhedron for Zn ‐ air batteries. Carbon Energy. 2020.

[102] Chen L, Huang B, Qiu X, Wang X, Luque R, Li Y. Seed-mediated growth of MOF-encapsulated Pd@Ag core–shell nanoparticles: toward advanced room temperature nanocatalysts. Chemical science. 2016;7:228-233.

[103] Chen L, Huang W, Wang X, Chen Z, Yang X, Luque R, Li Y. Catalytically active designer crown-jewel Pd-based nanostructures encapsulated in metal–organic frameworks. Chem. Commun. 2017;53:1184-1187.

[104] Luo T Y, Liu C, Gan X Y, Muldoon P F, Diemler N A, Millstone J E, Rosi N L. Multivariate Stratified Metal-Organic Frameworks: Diversification Using Domain Building Blocks. J. Am. Chem. Soc. 2019;141:2161-2168.

[105] Furukawa S, Hirai K, Nakagawa K, Takashima Y, Matsuda R, Tsuruoka T, Kondo M, Haruki R, Tanaka D, Sakamoto H. Heterogeneously hybridized porous coordination polymer crystals: fabrication of heterometallic core‐shell single crystals with an in‐plane rotational epitaxial relationship. Angew. Chem. 2009;121:1798-1802.

[106] Zeng T, Zhang X, Wang S, Niu H, Cai Y. Spatial Confinement of a Co3O4 Catalyst in Hollow Metal–Organic Frameworks as a Nanoreactor for Improved Degradation of Organic Pollutants. Environmental Science & Technology. 2015.

[107] Huang G, Zhang L, Zhang F, Wang L. Metal-organic framework derived Fe2O3@NiCo2O4 porous nanocages as anode materials for Li-ion batteries. Nanoscale. 2014;6:5509-5515.

[108] Huang G, Zhang F, Zhang L, Du X, Wang J, Wang L. Hierarchical NiFe2O4/Fe2O3 nanotubes derived from metal organic frameworks for superior lithium ion battery anodes. Journal of Materials Chemistry A. 2014;2:8048-8053.

[109] Huang Y-F, Sun X-Y, Huo S-H, Li Y, Zhong C. Core-shell dual-MOF heterostructures derived magnetic CoFe2O4/CuO (sub)microcages with superior catalytic performance. Appl. Surf. Sci. 2019;466:637-646.

[110] Aslam M K, Shah S S A, Li S, Chen C. Kinetically controlled synthesis of MOF nanostructures: single-holed hollow core-shell ZnCoS@Co9S8/NC for ultra-high performance lithium-ion batteries. Journal of Materials Chemistry A. 2018;6:14083-14090.

[111] Huang W, Zhang X, Zhao Y, Zhang J, Liu P. Hollow N-doped carbon polyhedrons embedded Co and Mo2C nanoparticles for high-efficiency and wideband microwave absorption. Carbon. 2020;167.

[112] Wang X, Yu L, Guan B Y, Song S, Lou X W. Metal-Organic Framework Hybrid-Assisted Formation of Co3O4 /Co-Fe Oxide Double-Shelled Nanoboxes for Enhanced Oxygen Evolution. Adv. Mater. 2018;30:1801211.

[113] Ahn, Wook, Park, Gyu M, Lee, Un D, Seo, Ho M, Jiang, Gaopeng. Hollow Multivoid Nanocuboids Derived from Ternary Ni-Co-Fe Prussian Blue Analog for Dual-Electrocatalysis of Oxygen and Hydrogen Evolution Reactions. Adv. Funct. Mater. 2018;1802129.

[114] Boissonnault J A, Wong-Foy A G, Matzger A J. Core-Shell Structures Arise Naturally During Ligand Exchange in Metal-Organic Frameworks. J. Am. Chem. Soc. 2017;139:14841-14844.

[115] Chen J, Ru Q, Mo Y, Hu S, Hou X. Design and synthesis of hollow NiCo2O4 nanoboxes as anodes for lithium-ion and sodium-ion batteries. PCCP. 2016;18:18949-18957.

[116] Xu W, Cui X, Xie Z, Dietrich G, Wang Y. Integrated Co3O4/TiO2 Composite Hollow Polyhedrons Prepared via Cation-exchange Metal-Organic Framework for Superior Lithium-ion Batteries. Electrochim. Acta. 2016;222:1021-1028.

[117] Hu H, Guan B, Xia B Y, Lou X W D. Designed Formation of Co3O4/NiCo2O4 Double-Shelled Nanocages with Enhanced Pseudocapacitive and Electrocatalytic Properties. J. Am. Chem. Soc. 2015;137:5590-5595.

[118] Zhang J, Hu H, Li Z, Lou X W D. Double‐Shelled Nanocages with Cobalt Hydroxide Inner Shell and Layered Double Hydroxides Outer Shell as High‐Efficiency Polysulfide Mediator for Lithium‐Sulfur Batteries. Angew. Chem. Int. Ed. 2016;55:3982-3986.

[119] Zhang L, Wu H B, Lou X W. Metal-organic-frameworks-derived general formation of hollow structures with high complexity. J. Am. Chem. Soc. 2013;44:no-no.

[120] Lyu F, Bai Y, Li Z, Xu W, Wang Q, Mao J, Wang L, Zhang X, Yi Y. Self-Templated Fabrication of CoO-MoO2 Nanocages for Enhanced Oxygen Evolution. Adv. Funct. Mater. 2017;27:1702324.

[121] Chen X-L, Huang J-W, Huang Y-C, Du J, Jiang Y-F, Zhao Y, Zhu H-B. Efficient Fe-Co-N-C Electrocatalyst Towards Oxygen Reduction Derived from a Cationic Co-II-based Metal-Organic Framework Modified by Anion-Exchange with Potassium Ferricyanide. Chemistry-an Asian Journal. 2019;14:995-1003.

[122] Lu Y, Yu L, Wu M, Wang Y, Lou X W. Construction of Complex Co3O4@Co3V2O8 Hollow Structures from Metal-Organic Frameworks with Enhanced Lithium Storage Properties. Adv. Mater. 2018;30.

[123] Morabito J V, Chou L Y, Li Z, Manna C M, Petroff C A, Kyada R J, Palomba J M, Byers J A, Tsung C K. Molecular Encapsulation beyond the Aperture Size Limit through Dissociative Linker Exchange in Metal-Organic Framework Crystals. J. Am. Chem. Soc. 2014;136:12540-12543.

[124] Abdelhamid H N, Huang Z, El-Zohry A M, Zheng H, Zou X. A Fast and Scalable Approach for Synthesis of Hierarchical Porous Zeolitic Imidazolate Frameworks and One-Pot Encapsulation of Target Molecules. Inorg. Chem. 2017;56:9139-9146.

[125] Dou L, Wu S, Chen D L, He S, Wang F F, Zhu W D. Structures and Electronic Properties of Au Clusters Encapsulated ZIF-8 and ZIF-90. The Journal of Physical Chemistry C. 2018;122:8901-8909.

[126] Zhou Y-H, Yang Q, Chen Y-Z, Jiang H-L. Low-cost CuNi@MIL-101 as an excellent catalyst toward cascade reaction: integration of ammonia borane dehydrogenation with nitroarene hydrogenation. Chem. Commun. 2017;53:12361-12364.

[127] Ying J, Yang X Y, Tian G, Janiak C, Su B L. Self-assembly: an option to nanoporous metal nanocrystals. Nanoscale. 2014;6:13370-13382.

[128] Ying, Jie, Li, Jing, Jiang, Gaopeng, Cano, Paul Z, Ma, Zhong. Metal-organic frameworks derived platinum-cobalt bimetallic nanoparticles in nitrogen-doped hollow porous carbon capsules as a highly active and durable catalyst for oxygen reduction reaction. Applied Catalysis B: Environmental. 2018;225:496-503.

[129] Liao Y T, Chi N V, Ishiguro N, Young A P, Wu C W. Engineering a Homogeneous Alloy-Oxide Interface Derived from Metal-Organic Frameworks for Selective Oxidation of 5-Hydroxymethylfurfural to 2,5-Furandicarboxylic Acid. Applied Catalysis B: Environmental. 2020;270:118805.

[130] Wu H B, Xia B Y, Yu L, Yu X Y, Lou X W. Porous molybdenum carbide nano-octahedrons synthesized via confined carburization in metal-organic frameworks for efficient hydrogen production. Nature Communications. 2015;6:6512.

[131] Tang Y J, Gao M R, Liu C H, Li S L, Jiang H L, Lan Y Q, Han M, Yu S H. Porous molybdenum‐based hybrid catalysts for highly efficient hydrogen evolution. Angew. Chem. 2015;127:13120-13124.

[132] Li J S, Tang Y J, Liu C H, Li S L, Li R H, Dong L Z, Dai Z H, Bao J C, Lan Y Q. Polyoxometalate-based metal–organic framework-derived hybrid electrocatalysts for highly efficient hydrogen evolution reaction. Journal of Materials Chemistry A. 2016;4.

[133] Tang Y J, Zhu H J, Dong L Z, Zhang A M, Li S L, Liu J, Lan Y Q. Solid-Phase Hot-Pressing of POMs-ZIFs Precursor and Derived Phosphide for Overall Water Splitting. Applied Catalysis B: Environmental. 2019;245:528-535.

[134] Chen G, Guo Z, Zhao W, Gao D, Li C, Ye C, Sun G. Design of Porous/Hollow Structured Ceria by Partial Thermal Decomposition of Ce-MOF and Selective Etching. Acs Appl Mater Interfaces. 2017;39594-39601.

[135] Zhou K, Tang D, Li W, Han Y, Chen M. Synergetic Lithium Storage of Bimetallic Sulfide Co8FeS8/N-C Dodecahedral Nanocages with Enhanced Lithium-ion Battery Performance. Chemical Engineering ence. 2019;208:115142.

[136] Hou C C, Zou L, Xu Q. A hydrangea‐like superstructure of open carbon cages with hierarchical porosity and highly active metal sites. Adv. Mater. 2019;31:1904689.

[137] Li T, Chen Y, Tang Z, Liu Z, Wang C. Palladium nanoparticles supported by metal-organic frameworks derived FeNi3Cx nanorods as efficient oxygen reversible catalysts for rechargeable Zn-Air batteries. Electrochim. Acta. 2019;307:403-413.

[138] Long X, Yin P, Lei T, Wang K, Zhan Z. Methanol electro-oxidation on Cu@Pt/C core-shell catalyst derived from Cu-MOF. Applied Catalysis B: Environmental. 2019;260:118187.

[139] Mandegarzad S, Raoof J B, Hosseini S R, Ojani R. MOF-derived Cu-Pd/nanoporous carbon composite as an efficient catalyst for hydrogen evolution reaction: A comparison between hydrothermal and electrochemical synthesis. Appl. Surf. Sci. 2018;436:451-459.

[140] Guo Z, Song L, Xu T, Gao D, Li C, Hu X, Chen G. CeO2-CuO Bimetal Oxides Derived from Ce-based MOF and Their Difference in Catalytic Activities for CO Oxidation. Mater. Chem. Phys. 2019;226:338-343.

[141] Huo M, Wang B, Zhang C, Ding S, Yuan H, Liang Z, Qi J, Chen M, Xu Y, Zhang W. 2D Metal–Organic Framework Derived CuCo Alloy Nanoparticles Encapsulated by Nitrogen‐Doped Carbonaceous Nanoleaves for Efficient Bifunctional Oxygen Electrocatalyst and Zinc–Air Batteries. Chemistry–A European Journal. 2019;25:12780-12788.

[142] Feng J X, Ye S H, Xu H, Tong Y X, Li G R. Design and Synthesis of FeOOH/CeO2 Heterolayered Nanotube Electrocatalysts for the Oxygen Evolution Reaction. Adv. Mater. 2016;28:4698-4703.

[143] Xu X, Tang J, Qian H, Hou S, Bando Y, Hossain M S A, Pan L, Yamauchi Y. Three-dimensional networked metal–organic frameworks with conductive polypyrrole tubes for flexible supercapacitors. ACS applied materials & interfaces. 2017;9:38737-38744.

[144] Kuang M, Wang Q, Ge H, Han P, Gu Z, Al-Enizi A M, Zheng G. CuCoOx/FeOOH Core-shell Nanowires as an Efficient Bifunctional Oxygen Evolution and Reduction Catalyst. Acs Energy Letters. 2017;2:2498-2505.

[145] Kuang M, Wang Q, Han P, Zheng G. Cu, Co‐embedded N‐enriched mesoporous carbon for efficient oxygen reduction and hydrogen evolution reactions. Advanced Energy Materials. 2017;7:1700193.

[146] Huo Q, Li J, Qi X, Liu G, Zhang X, Zhang B, Ning Y, Fu Y, Liu J, Liu S. Cu, Zn-embedded MOF-derived bimetallic porous carbon for adsorption desulfurization. Chem. Eng. J. 2019;378:122106.

[147] Zhao J, Li H, Li C, Zhang Q, Sun J, Wang X, Guo J, Xie L, Xie J, He B. MOF for template-directed growth of well-oriented nanowire hybrid arrays on carbon nanotube fibers for wearable electronics integrated with triboelectric nanogenerators. Nano Energy. 2018;45:420-431.

[148] Liu Z Q, Cheng H, Li N, Ma T Y, Su Y Z. ZnCo2O4 Quantum Dots Anchored on Nitrogen‐Doped Carbon Nanotubes as Reversible Oxygen Reduction/Evolution Electrocatalysts. Adv. Mater. 2016;28:3777-3784.

[149] Peng S, Li L, Han X, Sun W, Srinivasan M, Mhaisalkar S G, Cheng F, Yan Q, Chen J, Ramakrishna S. Cobalt sulfide nanosheet/graphene/carbon nanotube nanocomposites as flexible electrodes for hydrogen evolution. Angew. Chem. 2014;126:12802-12807.

[150] Song B, Zeng Z, Zeng G, Gong J, Xiao R, Chen M, Tang X, Ye S, Shen M. Effects of hydroxyl, carboxyl, and amino functionalized carbon nanotubes on the functional diversity of microbial community in riverine sediment. Chemosphere. 2021;262:128053.

[151] Wang X, Huang F, Rong F, He P, Que R. Unique MOF-derived hierarchical MnO2 nanotubes@NiCo-LDH/CoS2 nanocage materials as high performance supercapacitors. Journal of Materials Chemistry A. 2019;7:12018-12028.

[152] Guo M, Li Y, Zhou L, Zheng Q, Jie W, Xie F, Xu C, Lin D. Hierarchically structured bimetallic electrocatalyst synthesized via template-directed fabrication MOF arrays for high-efficiency oxygen evolution reaction. Electrochim. Acta. 2018;298:525-532.

[153] Xun S, Xu Y, He J, Jiang D, Yang R, Li D, Chen M. MOF-derived cobalt oxides nanoparticles anchored on CoMoO4 as a highly active electrocatalyst for oxygen evolution reaction. J. Alloys Compd. 2019;806:1097-1104.

[154] Sun T, Xu L, Wang D, Li Y. Metal organic frameworks derived single atom catalysts for electrocatalytic energy conversion. Nano research. 2019;12:2067-2080.

[155] Das S, Pérez-Ramírez J, Gong J, Dewangan N, Hidajat K, Gates B C, Kawi S. Core-shell structured catalysts for thermocatalytic, photocatalytic, and electrocatalytic conversion of CO2. Chem. Soc. Rev. 2020;49:2937-3004.

[156] Sun Y, Xu S, Ortíz-Ledón C A, Zhu J, Chen S, Duan J. Biomimetic assembly to superplastic metal–organic framework aerogels for hydrogen evolution from seawater electrolysis. Exploration. 2021;1:20210021.

[157] Yan W, Cao X, Wang R, Sha Y, Cui P, Cui S. S, N co-doped rod-like porous carbon derived from S, N organic ligand assembled Ni-MOF as an efficient electrocatalyst for oxygen reduction reaction. J. Solid State Chem. 2019;275:167-173.

[158] Asano M, Kawamura R, Sasakawa R, Todoroki N, Wadayama T. Oxygen Reduction Reaction Activity for Strain-Controlled Pt-Based Model Alloy Catalysts: Surface Strains and Direct Electronic Effects Induced by Alloying Elements. Acs Catalysis. 2016;6:5285-5289.

[159] Wei J, Hu Y, Liang Y, Kong B, Zheng Z, Zhang J, Jiang S P, Zhao Y, Wang H. Graphene oxide/core-shell structured metal-organic framework nano-sandwiches and their derived cobalt/N-doped carbon nanosheets for oxygen reduction reactions. Journal of Materials Chemistry A. 2017;5:10182-10189.

[160] Li L, Larsen A H, Romero N A, Morozov V A, Glinsvad C, Abild-Pedersen F, Greeley J, Jacobsen K W, Nørskov J K. Investigation of catalytic finite-size-effects of platinum metal clusters. The journal of physical chemistry letters. 2013;4:222-226.

[161] Yin P, Yao T, Wu Y, Zheng L, Lin Y, Liu W, Ju H, Zhu J, Hong X, Deng Z. Single cobalt atoms with precise N ‐ coordination as superior oxygen reduction reaction catalysts. Angew. Chem. 2016;128:10958-10963.

[162] Gao Y, Wu T, Yang C, Ma C, Zhao Z, Wu Z, Cao S, Geng W, Wang Y, Yao Y, Zhang Y, Cheng C. Activity Trends and Mechanisms in Peroxymonosulfate-Assisted Catalytic Production of Singlet Oxygen over Atomic Metal-N-C Catalysts. Angewandte Chemie-International Edition. 2021;60:22513-22521.

[163] Zhang L, Fischer J M T A, Jia Y, Yan X, Xu W, Wang X, Chen J, Yang D, Liu H, Zhuang L, Hankel M, Searles D J, Huang K, Feng S, Brown C L, Yao X. Coordination of Atomic Co-Pt Coupling Species at Carbon Defects as Active Sites for Oxygen Reduction Reaction. J. Am. Chem. Soc. 2018;140:10757-10763.

[164] Lai W H, Zhang B W, Hu Z, Qu X M, Jiang Y X, Wang Y X, Wang J Z, Liu H K, Chou S L. The Quasi-Pt-Allotrope Catalyst: Hollow PtCo@single-Atom Pt-1 on Nitrogen-Doped Carbon toward Superior Oxygen Reduction. Adv. Funct. Mater. 2019;29:1807340.

[165] Hassan D, El-Safty S, Khalil K A, Dewidar M, Abu El-magd G. Carbon supported engineering NiCo2O4 hybrid nanofibers with enhanced electrocatalytic activity for oxygen reduction reaction. Materials. 2016;9:759.

[166] Meng Z, Cai S, Wang R, Tang H, Song S, Tsiakaras P. Bimetallic-organic framework-derived hierarchically porous Co-Zn-N-C as efficient catalyst for acidic oxygen reduction reaction. Applied Catalysis B: Environmental. 2019;244:120-127.

[167] Wang J, Lu H, Hong Q, Cao Y, Li X, Bai J. Porous N, S-codoped carbon architectures with bimetallic sulphide nanoparticles encapsulated in graphitic layers: highly active and robust electrocatalysts for the oxygen reduction reaction in Al-air batteries. Chem. Eng. J. 2017;330:1342-1350.

[168] Yan H, Xie Y, Wu A, Cai Z, Wang L, Tian C, Zhang X, Fu H. Anion-Modulated HER and OER Activities of 3D Ni-V-Based Interstitial Compound Heterojunctions for High-Efficiency and Stable Overall Water Splitting. Adv. Mater. 2019;31.

[169] Wang W, Yang Y, Huan D, Wang L, Shi N, Xie Y, Xia C, Peng R, Lu Y. An excellent OER electrocatalyst of cubic SrCoO3- prepared by a simple F-doping strategy. Journal of Materials Chemistry A. 2019;7:12538-12546.

[170] Antony R P, Satpati A K, Bhattacharyya K, Jagatap B N. MOF Derived Nonstoichiometric $Ni_xCo_{3-x}O_{4-y}$ Nanocage for Superior Electrocatalytic Oxygen Evolution. Advanced Materials Interfaces. 2016;3:1600632.

[171] Liu T, Yang F, Cheng G, Luo W. Reduced Graphene Oxide‐Wrapped Co9‐xFexS8/Co, Fe‐N‐C Composite as Bifunctional Electrocatalyst for Oxygen Reduction and Evolution. Small. 2018;14:1703748.

[172] Li H, Chen S, Zhang Y, Zhang Q, Jia X, Zhang Q, Gu L, Sun X, Song L, Wang X. Systematic design of superaerophobic nanotube-array electrode comprised of transition-metal sulfides for overall water splitting. Nature communications. 2018;9:1-12.

[173] Wang B, Chen Y, Wang X, Zhang X, Hu Y, Yu B, Yang D, Zhang W. A microwave-assisted bubble bursting strategy to grow Co8FeS8/CoS heterostructure on rearranged carbon nanotubes as efficient electrocatalyst for oxygen evolution reaction. J. Power Sources. 2020;449:227561.

[174] Li G, Zhang X, Zhang H. Ultrathin 2D Nanosheet Based 3D Hierarchical Hollow Polyhedral CoM/C (M = Ni, Cu, Mn) Phosphide Nanocages as Superior Electrocatalysts toward Oxygen Evolution Reaction. Chem. Eng. J. 2020;125467.

[175] Huang H, Yu C, Yang J, Zhao C, Han X, Liu Z, Qiu J. Strongly coupled architectures of cobalt phosphide nanoparticles assembled on graphene as bifunctional electrocatalysts for water splitting. ChemElectroChem. 2016;3:719-725.

[176] Tan Y, Wang H, Liu P, Shen Y, Cheng C, Hirata A, Fujita T, Tang Z, Chen M. Versatile nanoporous bimetallic phosphides towards electrochemical water splitting. Energy & Environmental Science. 2016;9:2257-2261.

[177] Li Z, Zhao T-T, Jiang W-J, Niu S, Wu M, Hu J-S. Bimetal Prussian Blue as a Continuously Variable Platform for Investigating the Composition-Activity Relationship of Phosphides-Based Electrocatalysts for Water Oxidation. Acs Applied Materials & Interfaces. 2018;10:35904-35910.

[178] He P, Yu X Y, Lou X W. Carbon‐incorporated nickel–cobalt mixed metal phosphide nanoboxes with enhanced electrocatalytic activity for oxygen evolution. Angew. Chem. Int. Ed. 2017;56:3897-3900.

[179] Zheng Y, Jiao Y, Vasileff A, Qiao S-Z. The Hydrogen Evolution Reaction in Alkaline Solution: From Theory, Single Crystal Models, to Practical Electrocatalysts. Angewandte Chemie-International Edition. 2018;57:7568-7579.

[180] Sun X, Dai J, Guo Y, Wu C, Hu F, Zhao J, Zeng X, Xie Y. Semimetallic molybdenum disulfide ultrathin nanosheets as an efficient electrocatalyst for hydrogen evolution. Nanoscale. 2014;6:8359-8367.

[181] Zhang Z, Li W, Yuen M F, Ng T-W, Tang Y, Lee C-S, Chen X, Zhang W. Hierarchical composite structure of few-layers MoS2 nanosheets supported by vertical graphene on carbon cloth for high-performance hydrogen evolution reaction. Nano Energy. 2015;18:196-204.

[182] Jaramillo T F, Jørgensen K P, Bonde J, Nielsen J H, Horch S, Chorkendorff I. Identification of active edge sites for electrochemical H-2 evolution from MoS2 nanocatalysts. science. 2007;317:100-102.

[183] Yu X Y, Feng Y, Jeon Y, Guan B, Lou X W, Paik U. Formation of Ni–Co–MoS2 nanoboxes with enhanced electrocatalytic activity for hydrogen evolution. Adv. Mater. 2016;28:9006-9011.

[184] Guo Y, Tang J, Qian H, Wang Z, Yamauchi Y. One-pot synthesis of zeolitic imidazolate framework 67-derived hollow Co3S4@ MoS2 heterostructures as efficient bifunctional catalysts. Chem. Mater. 2017;29:5566-5573.

[185] Zhang B, Xiao C, Xie S, Liang J, Chen X, Tang Y. Iron–nickel nitride nanostructures in situ grown on surface-redox-etching nickel foam: efficient and ultrasustainable electrocatalysts for overall water splitting. Chem. Mater. 2016;28:6934-6941.

[186] Jia X, Zhao Y, Chen G, Shang L, Shi R, Kang X, Waterhouse G I, Wu L Z, Tung C H, Zhang T. Ni3FeN nanoparticles derived from ultrathin NiFe‐layered double hydroxide nanosheets: an efficient overall water splitting electrocatalyst. Advanced Energy Materials. 2016;6:1502585.

[187] Zhang Y, Ouyang B, Xu J, Chen S, Rawat R S, Fan H J. 3D Porous Hierarchical Nickel-Molybdenum Nitrides Synthesized by RF Plasma as Highly Active and Stable Hydrogen-Evolution-Reaction Electrocatalysts. Advanced Energy Materials. 2016;6:1600221.

[188] Feng X, Wang H, Bo X, Guo L. Bimetal–Organic framework-derived porous rodlike cobalt/nickel nitride for all-pH value electrochemical hydrogen evolution. ACS applied materials & interfaces. 2019;11:8018-8024.

[189] Li S, Zhang Q, Sun J, Guan J. Favorable role of heterojunction in trimetallic Fe–Co–Cu phosphides on nitrogen-doped carbon materials for hydrogen evolution. Materials Today Energy. 2020;17:100464.

[190] Yan L, Cao L, Dai P, Gu X, Liu D, Li L, Wang Y, Zhao X. Metal‐organic frameworks derived nanotube of nickel–cobalt bimetal phosphides as highly efficient electrocatalysts for overall water splitting. Adv. Funct. Mater. 2017;27:1703455.

[191] Chen B, Kim D, Zhang Z, Lee M, Yong K. MOF-Derived NiCoZnP Nanoclusters Anchored on Hierarchical N-doped Carbon Nanosheets Array as Bifunctional Electrocatalysts for Overall Water Splitting. Chem. Eng. J. 2021;422:130533.

[192] Shi J, Qiu F, Yuan W, Guo M, Lu Z-H. Nitrogen-doped carbon-decorated yolk-shell CoP@FeCoP micro-polyhedra derived from MOF for efficient overall water splitting. Chem. Eng. J. 2021;403:126312.

[193] Patil S J, Chodankar N R, Hwang S-K, Shinde P A, Raju G S R, Ranjith K S, Huh Y S, Han Y-K. Co-metal–organic framework derived CoSe2@MoSe2 core–shell structure on carbon cloth as an efficient bifunctional catalyst for overall water splitting. Chem. Eng. J. 2022;429:132379.

[194] Wei L, Karahan H E, Zhai S, Liu H, Chen X, Zhou Z, Lei Y, Liu Z, Chen Y. Amorphous bimetallic oxide–graphene hybrids as bifunctional oxygen electrocatalysts for rechargeable Zn–air batteries. Adv. Mater. 2017;29:1701410.

[195] Feng C, Guo Y, Xie Y, Cao X, Li S, Zhang L, Wang W, Wang J. Bamboo-like nitrogen-doped porous carbon nanofibers encapsulated nickel-cobalt alloy nanoparticles composite material derived from the electrospun fiber of a bimetal-organic framework as efficient bifunctional oxygen electrocatalysts. Nanoscale. 2020;12:5942-5952.

[196] Han X, Ling X, Yu D, Xie D, Li L, Peng S, Zhong C, Zhao N, Deng Y, Hu W. Atomically Dispersed Binary Co-Ni Sites in Nitrogen-Doped Hollow Carbon Nanocubes for Reversible Oxygen Reduction and Evolution. Adv. Mater. 2019;31:e1905622.

[197] Ren J T, Wang Y S, Chen L, Gao L J, Tian W W, Yuan Z Y. Binary FeNi phosphides dispersed on N,P-doped carbon nanosheets for highly efficient overall water splitting and rechargeable Zn-air batteries. Chem. Eng. J. 2020;389:124408.

[198] Gu T, Sa R, Zhang L, Li D-S, Wang R. Engineering interfacial coupling between Mo2C nanosheets and Co@NC polyhedron for boosting electrocatalytic water splitting and zinc-air batteries. Applied Catalysis B: Environmental. 2021;296:120360.

[199] Vijayakumar E, Ramakrishnan S, Sathiskumar C, Yoo D J, Balamurugan J, Noh H S, Kwon D, Kim Y H, Lee H. MOF-derived CoP-nitrogen-doped carbon@NiFeP nanoflakes as an efficient and durable electrocatalyst with multiple catalytically active sites for OER, HER, ORR and rechargeable zinc-air batteries. Chem. Eng. J. 2022;428:131115.

[200] Xu Z, Liang Z, Guo W, Zou R. In situ/operando vibrational spectroscopy for the investigation of advanced nanostructured electrocatalysts. Coord. Chem. Rev. 2021;436.

[201] Goerlin M, Chernev P, de Araujo J F, Reier T, Dresp S, Paul B, Kraehnert R, Dau H, Strasser P. Oxygen Evolution Reaction Dynamics, Faradaic Charge Efficiency, and the Active Metal Redox States of Ni-Fe Oxide Water Splitting Electrocatalysts. J. Am. Chem. Soc. 2016;138:5603-5614.

[202] Wang D, Zhou J, Hu Y, Yang J, Han N, Li Y, Sham T-K. In Situ X-ray Absorption Near-Edge Structure Study of Advanced NiFe(OH)(x) Electrocatalyst on

Carbon Paper for Water Oxidation. Journal of Physical Chemistry C. 2015;119:19573-19583.

[203] Xiang W, Yang N, Li X, Linnemann J, Hagemann U, Ruediger O, Heidelmann M, Falk T, Aramini M, DeBeer S, Muhler M, Tschulik K, Li T. 3D atomic-scale imaging of mixed Co-Fe spinel oxide nanoparticles during oxygen evolution reaction. Nature communications. 2022;13:179-179.

[204] Nayak S, McPherson I J, Vincent K A. Adsorbed Intermediates in Oxygen Reduction on Platinum Nanoparticles Observed by In Situ IR Spectroscopy. Angewandte Chemie-International Edition. 2018;57:12855-12858.

[205] Wang H-Y, Hsu Y-Y, Chen R, Chan T-S, Chen H M, Liu B. Ni3+-Induced Formation of Active NiOOH on the Spinel Ni-Co Oxide Surface for Efficient Oxygen Evolution Reaction. Advanced Energy Materials. 2015;5.

[206] Gao M-R, Liang J-X, Zheng Y-R, Xu Y-F, Jiang J, Gao Q, Li J, Yu S-H. An efficient molybdenum disulfide/cobalt diselenide hybrid catalyst for electrochemical hydrogen generation. Nature Communications. 2015;6.

[207] Li Y, Zhang H, Jiang M, Zhang Q, He P, Sun X. 3D Self-Supported Fe-Doped Ni2P Nanosheet Arrays as Bifunctional Catalysts for Overall Water Splitting. Adv. Funct. Mater. 2017;27.

[208] Friebel D, Louie M W, Bajdich M, Sanwald K E, Cai Y, Wise A M, Cheng M-J, Sokaras D, Weng T-C, Alonso-Mori R, Davis R C, Bargar J R, Norskov J K, Nilsson A, Bell A T. Identification of Highly Active Fe Sites in (Ni,Fe)OOH for Electrocatalytic Water Splitting. J. Am. Chem. Soc. 2015;137:1305-1313.

[209] Hoskins B F, Robson R. Infinite polymeric frameworks consisting of three dimensionally linked rod-like segments. J. Am. Chem. Soc. 1989;111:5962-5964.

[210] Liu B, Shioyama H, Akita T, Xu Q. Metal-organic framework as a template for porous carbon synthesis. J. Am. Chem. Soc. 2008;130:5390-+.

[211] Zou F, Hu X, Li Z, Qie L, Hu C, Zeng R, Jiang Y, Huang Y. MOF-Derived Porous ZnO/ZnFe2O4/C Octahedra with Hollow Interiors for High-Rate Lithium-Ion Batteries. Adv. Mater. 2014;26:6622-6628.

[212] Xi J, Xia Y, Xu Y, Xiao J, Wang S. (Fe,Co)@nitrogen-doped graphitic carbon nanocubes derived from polydopamine-encapsulated metal-organic frameworks as a highly stable and selective non-precious oxygen reduction electrocatalyst. Chem. Commun. 2015;51:10479-10482.

[213] Hao J, Yang W, Zhang Z, Tang J. Metal-organic frameworks derived CoxFe1-xP nanocubes for electrochemical hydrogen evolution. Nanoscale. 2015;7:11055-11062.

[214] Yang Y, Lun Z, Xia G, Zheng F, He M, Chen Q. Non-precious alloy encapsulated in nitrogen-doped graphene layers derived from MOFs as an active and durable hydrogen evolution reaction catalyst. Energy & Environmental Science. 2015;8:3563-3571.

[215] Dong Q, Wang Q, Dai Z, Qiu H, Dong X. MOF-Derived Zn-Doped CoSe2 as an Efficient and Stable Free-Standing Catalyst for Oxygen Evolution Reaction. Acs Applied Materials & Interfaces. 2016;8:26902-26907.

[216] Ming F, Liang H, Shi H, Xu X, Mei G, Wang Z. MOF-derived Co-doped nickel selenide/C electrocatalysts supported on Ni foam for overall water splitting. Journal of Materials Chemistry A. 2016;4:15148-15155.

[217] Fan L, Liu P F, Yan X, Gu L, Yang Z Z, Yang H G, Qiu S, Yao X. Atomically isolated nickel species anchored on graphitized carbon for efficient hydrogen evolution electrocatalysis. Nature Communications. 2016;7.

[218] Wang J, Huang Z, Liu W, Chang C, Tang H, Li Z, Chen W, Jia C, Yao T, Wei S, Wu Y, Lie Y. Design of N-Coordinated Dual-Metal Sites: A Stable and Active Pt-Free Catalyst for Acidic Oxygen Reduction Reaction. J. Am. Chem. Soc. 2017;139:17281-17284.

[219] Yang Y, Lin Z, Gao S, Su J, Lun Z, Xia G, Chen J, Zhang R, Chen Q. Tuning Electronic Structures of Nonprecious Ternary Alloys Encapsulated in Graphene Layers for Optimizing Overall Water Splitting Activity. Acs Catalysis. 2017;7:469-479.

[220] Wang X, Yu L, Guan B Y, Song S, Lou X W. Metal-Organic Framework Hybrid-Assisted Formation of Co3O4/Co-Fe Oxide Double-Shelled Nanoboxes for Enhanced Oxygen Evolution. Adv. Mater. 2018;30.

[221] Zhang L, Fischer J M T A, Jia Y, Yan X, Xu W, Wang X, Chen J, Yang D, Liu H, Zhuang L, Hanke M, Searles D J, Huang K, Feng S, Brown C L, Yao X. Coordination of Atomic Co-Pt Coupling Species at Carbon Defects as Active Sites for Oxygen Reduction Reaction. J. Am. Chem. Soc. 2018;140:10757-10763.

[222] Yang D, Su Z, Chen Y, Srinivas K, Zhang X, Zhang W, Lin H. Self-reconstruction of a MOF-derived chromium-doped nickel disulfide in electrocatalytic water oxidation. Chem. Eng. J. 2022;430.

[223] Feng Y, Yu X-Y, Paik U. N-doped graphene layers encapsulated NiFe alloy nanoparticles derived from MOFs with superior electrochemical performance for oxygen evolution reaction. Scientific Reports. 2016;6.

[224] Xiao X, He C-T, Zhao S, Li J, Lin W, Yuan Z, Zhang Q, Wang S, Dai L, Yu D. A general approach to cobalt-based homobimetallic phosphide ultrathin nanosheets for highly efficient oxygen evolution in alkaline media. Energy & Environmental Science. 2017;10:893-899.

[225] Antony R P, Satpati A K, Bhattacharyya K, Jagatap B N. MOF Derived Nonstoichiometric NixCo3-xO4-y Nanocage for Superior Electrocatalytic Oxygen Evolution. Advanced Materials Interfaces. 2016;3.

[226] Niu Y, Qian X, Xu C, Liu H, Wu W, Hou L. Cu-Ni-CoSex quaternary porous nanocubes as enhanced Pt-free electrocatalysts for highly efficient dye-sensitized solar cells and hydrogen evolution in alkaline medium. Chem. Eng. J. 2019;357:11-20.

[227] Feng Y, Yu X-Y, Paik U. Nickel cobalt phosphides quasi-hollow nanocubes as an efficient electrocatalyst for hydrogen evolution in alkaline solution. Chem. Commun. 2016;52:1633-1636.

[228] Guo X, Yu X, Feng Z, Liang J, Li Q, Lv Z, Liu B, Hao C, Li G. Intercalation Synthesis of Prussian Blue Analogue Nanocone and Their Conversion into Fe-Doped CoxP Nanocone for Enhanced Hydrogen Evolution. Acs Sustainable Chemistry & Engineering. 2018;6:8150-8158.

[229] Wu S, Shen X, Zhu G, Zhou E, Ji Z, Ma L, Xu K, Yang J, Yuan A. Metal organic framework derived NiFe@N-doped graphene microtube composites for hydrogen evolution catalyst. Carbon. 2017;116:68-76.

[230] Chen J, Yang Y, Su J, Jiang P, Xia C, Chen Q. Enhanced Activity for Hydrogen Evolution Reaction over CoFe Catalysts by Alloying with Small Amount of Pt. Acs Applied Materials & Interfaces. 2017;9:3596-3601.

[231] Agarwal S, Yu X, Manthiram A. A pair of metal organic framework (MOF)-derived oxygen reduction reaction (ORR) and oxygen evolution reaction (OER) catalysts for zinc-air batteries. Materials Today Energy. 2020;16.

[232] Guan B Y, Lu Y, Wang Y, Wu M, Lou X W D. Porous Iron-Cobalt Alloy/Nitrogen-Doped Carbon Cages Synthesized via Pyrolysis of Complex Metal-Organic Framework Hybrids for Oxygen Reduction. Adv. Funct. Mater. 2018;28:1706738.

[233] Zhao R, Liang Z, Gao S, Yang C, Zhu B, Zhao J, Qu C, Zou R, Xu Q. Puffing up energetic metal–organic frameworks to large carbon networks with hierarchical porosity and atomically dispersed metal sites. Angew. Chem. 2019;58:1975-1979.

[234] Ahn S H, Manthiram A. Direct growth of ternary Ni-Fe-P porous nanorods onto nickel foam as a highly active, robust bi-functional electrocatalyst for overall water splitting. Journal of Materials Chemistry A. 2017;5:2496-2503.

[235] Song J, Zhu C, Xu B Z, Fu S, Engelhard M H, Ye R, Du D, Beckman S P, Lin Y. Bimetallic cobalt ‐ based phosphide zeolitic imidazolate framework: CoPx phase ‐ dependent electrical conductivity and hydrogen atom adsorption energy for efficient overall water splitting. Advanced Energy Materials. 2017;7:1601555.

[236] Ren S, Duan X, Ge F, Chen Z, Yang Q, Zhang M, Zheng H. Novel MOF-derived hollow CoFe alloy coupled with N-doped Ketjen Black as boosted bifunctional oxygen catalysts for Zn-air batteries. Chem. Eng. J. 2022;427.

[237] Li Y-y, Zou Q, Li Z, Xie D, Niu Y, Zou J, Zeng X, Huang J. MOF derived Ni-Fe based alloy carbon materials for efficient bifunctional electrocatalysts applied in Zn-air battery. Appl. Surf. Sci. 2022;572.

[238] Ren D, Ying J, Xiao M, Deng Y-P, Ou J, Zhu J, Liu G, Pei Y, Li S, Jauhar A M, Jin H, Wang S, Su D, Yu A, Chen Z. Hierarchically Porous Multimetal-Based Carbon Nanorod Hybrid as an Efficient Oxygen Catalyst for Rechargeable Zinc-Air Batteries. Adv. Funct. Mater. 2020;30.

[239] Vijayakuma E, Ramakrishnan S, Sathiskumar C, Yoo D J, Balamurugan J, Noh H S, Kwon D, Kim Y H, Lee H. MOF-derived CoP-nitrogen-doped carbon@NiFeP nanoflakes as an efficient and durable electrocatalyst with multiple catalytically active sites for OER, HER, ORR and rechargeable zinc-air batteries. Chem. Eng. J. 2022;428.

[240] Chen B, Ma G, Zhu Y, Wang J, Xiong W, Xia Y. Metal-organic-framework-derived bi-metallic sulfide on N, S-codoped porous carbon nanocomposites as multifunctional electrocatalysts. J. Power Sources. 2016;334:112-119.

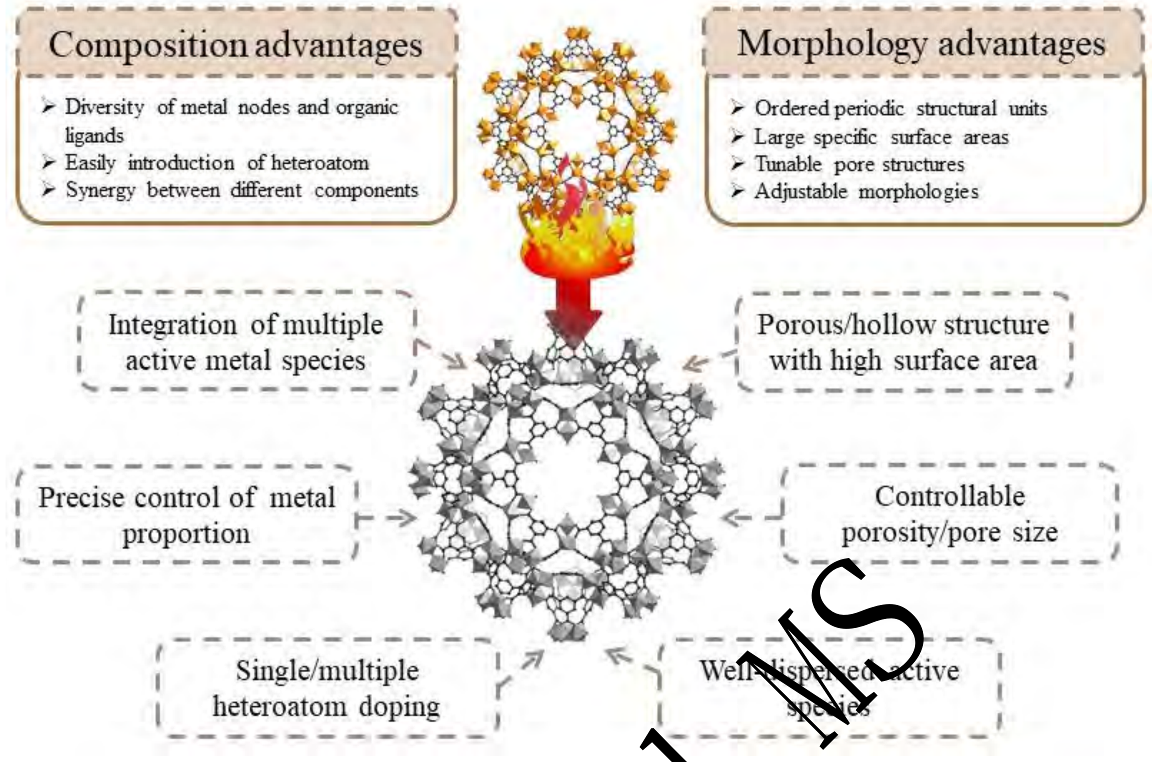

Fig. 1. The advantages of using MOFs as precursors/templates to prepare multi-metallic nanomaterials.

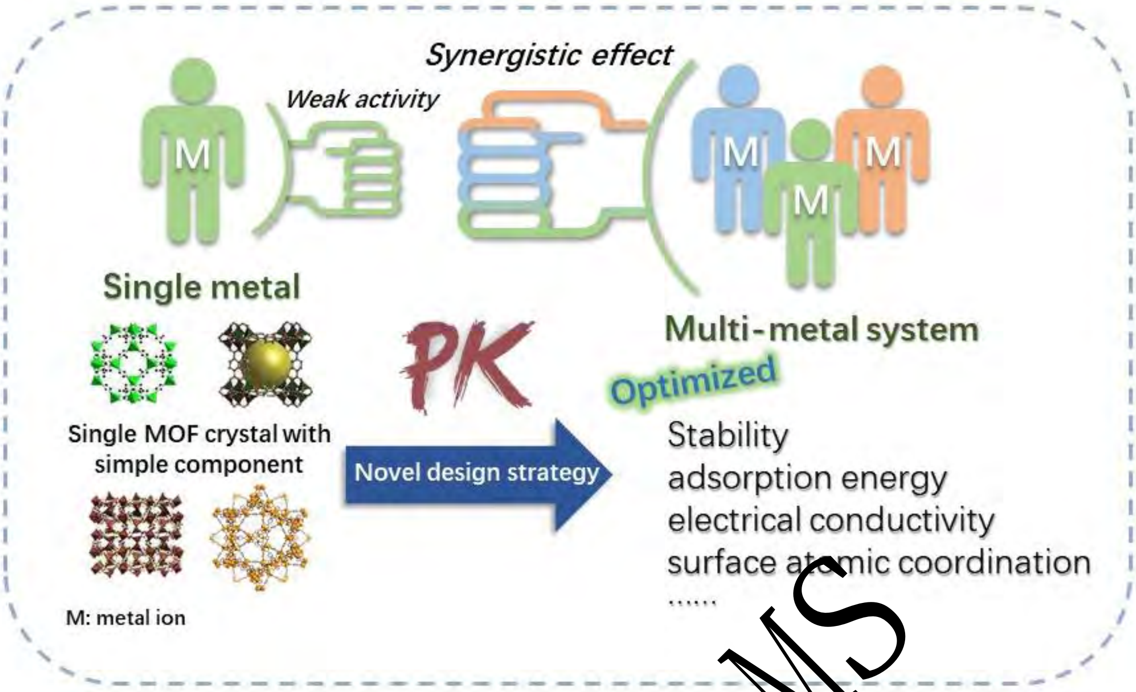

Fig. 2. The schematic of the advantages of MOF-derived multi-metal system in electrocatalysis compared with their monometallic counterparts.

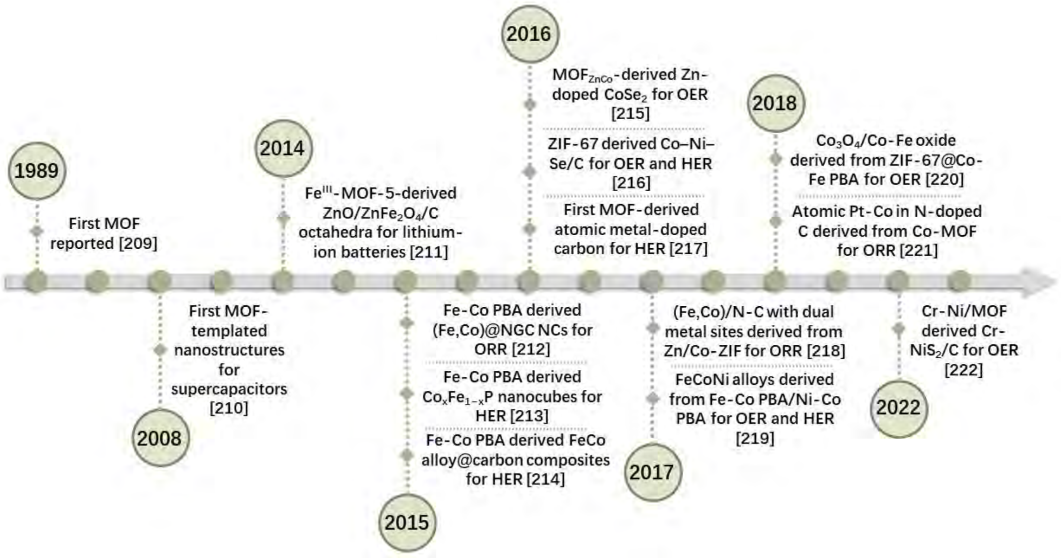

Fig. 3. Developmental milestones of MOFs and MOF-based multi-metallic nanomaterials for electrocatalytic applications [209-222].

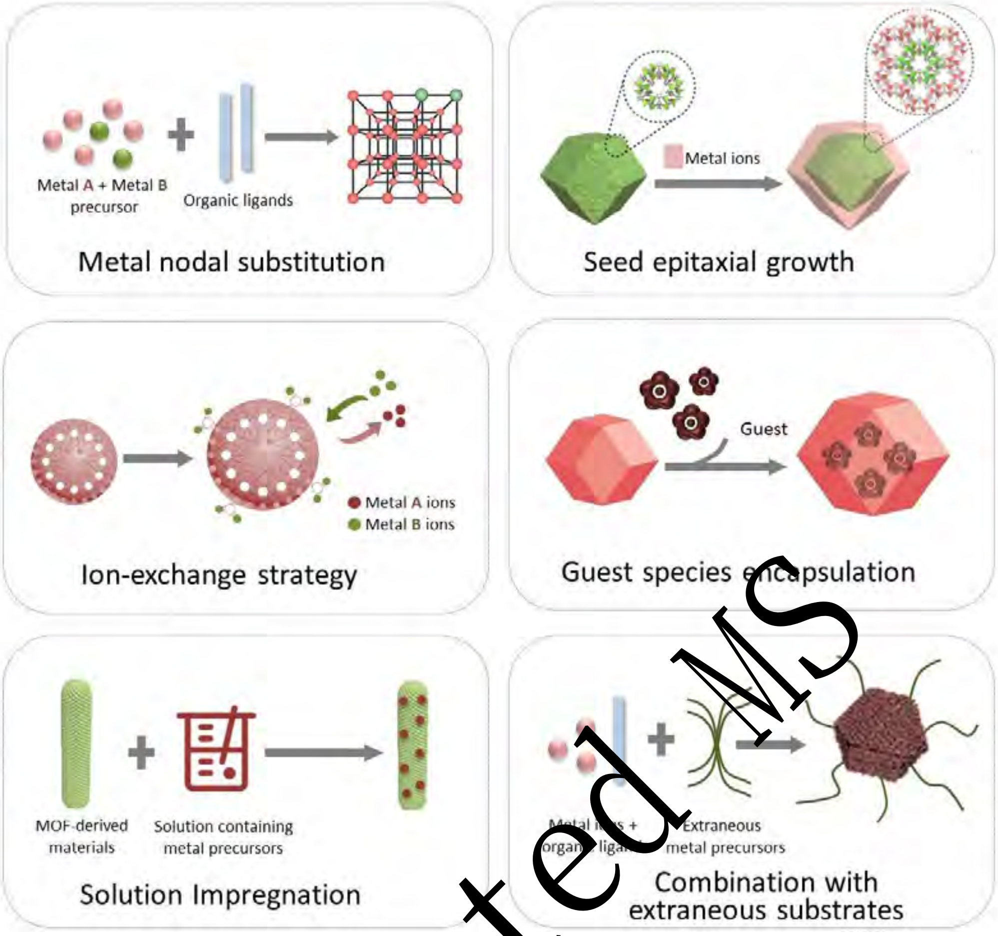

Fig. 4. Summary of the design strategies of multi-metallic MOF precursors.

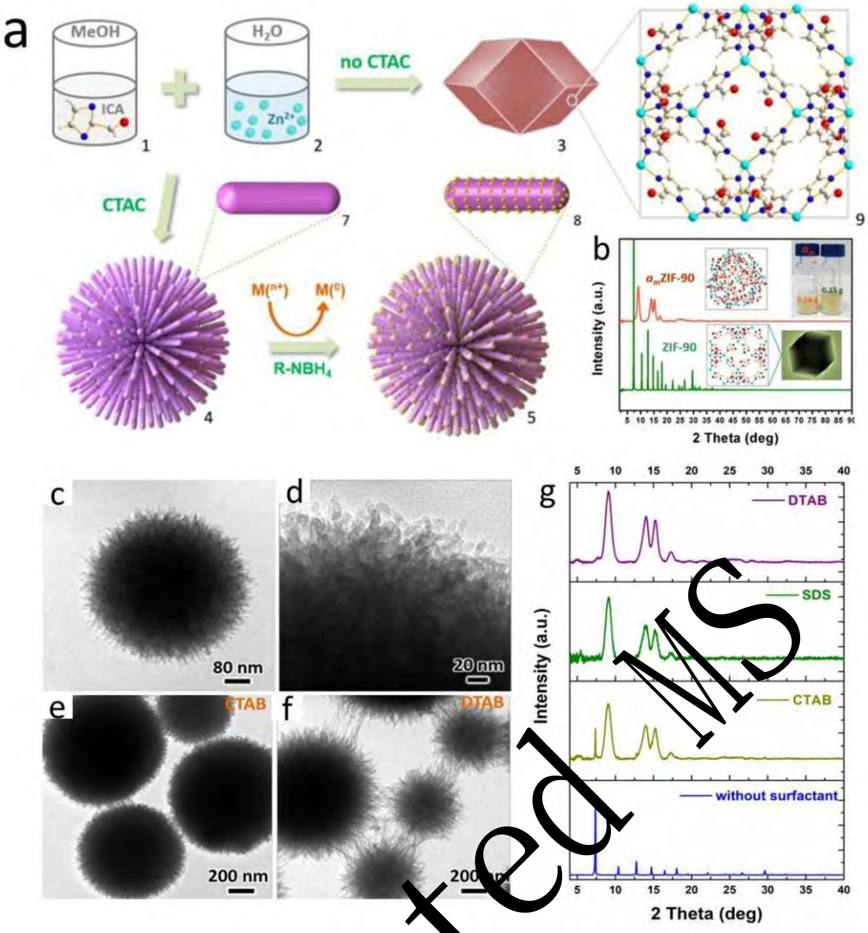

Fig. 5. a) Schematic illustration of the preparation of crystalline ZIF-90 and $_{\text{am}}$ZIF-90. b) XRD patterns of amorphous $_{\text{am}}$ZIF-90 and crystalline ZIF-90. c, d) TEM images of $_{\text{am}}$ZIF-90. TEM images of the products prepared by using e) CTAB and f) DTAB surfactants. g) XRD patterns of the ZIF-90 related products prepared by using different surfactants. Reproduced with permission.[97] Copyright 2017, American Chemical Society.

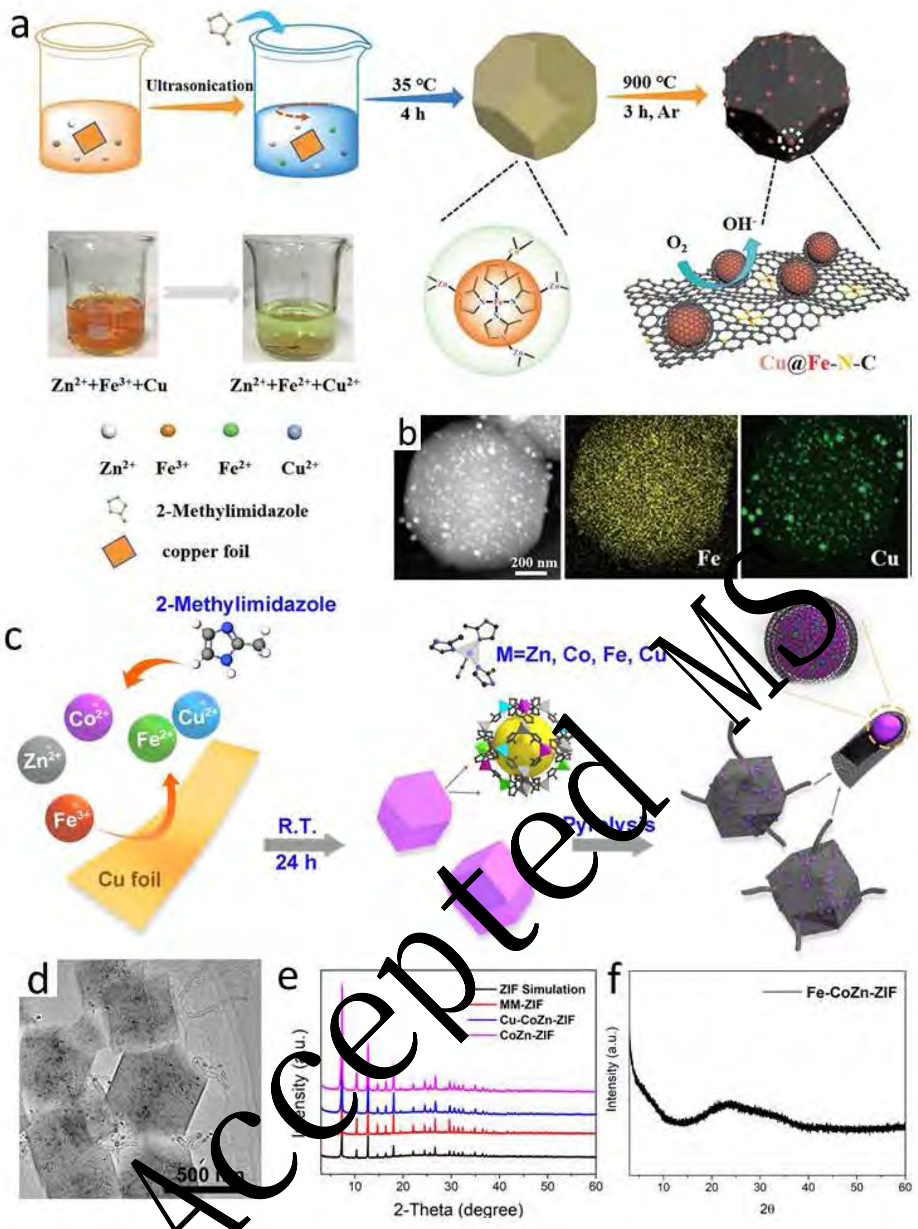

Fig. 6. a) Schematic of the synthesis procedure of Cu@Fe-N-C. b) Elemental mappings of Cu@Fe-N-C. Reproduced with permission.[100] Copyright 2018, Wiley VCH. c) Schematic illustration of the synthetic strategy of FC-C@NC. d) TEM image of FC-C@NC. e) XRD patterns of different samples. f) PXRD of the directly synthesized Fe-CoZn-ZIF in the ambient atmosphere via the co-precipitation. Reproduced with permission.[101] Copyright 2020, Wiley VCH.

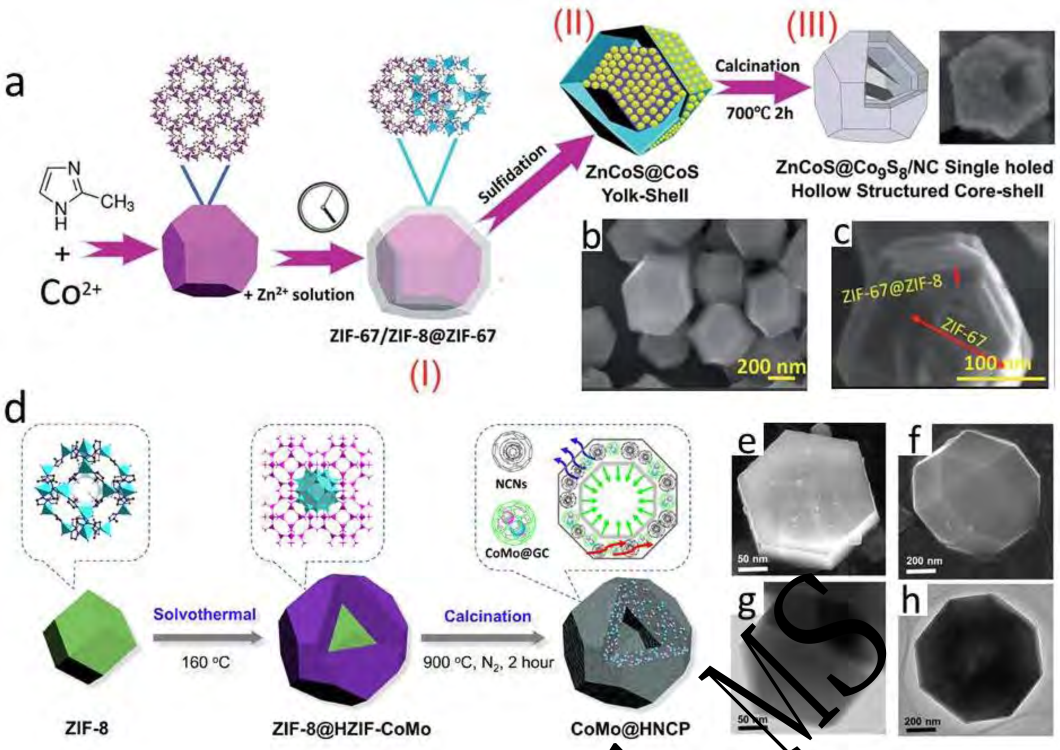

Fig. 7. a) Schematic illustration of the formation process of single-holed hollow core–shell ZnCoS@$Co_9S_8$/NC. b, c) Field emission SEM images of as prepared ZIF-67/ZIF-8@ZIF-67. Reproduced with permission.[110] Copyright 2018, The Royal Society of Chemistry. d) Schematic illustration for the synthesis process of hollow CoMo@HNCP polyhedron. SEM and TEM images of e, g) ZIF-8 and f, h) ZIF-8@HZIF-CoMo. Reproduced with permission.[111] Copyright 2020, Elsevier.

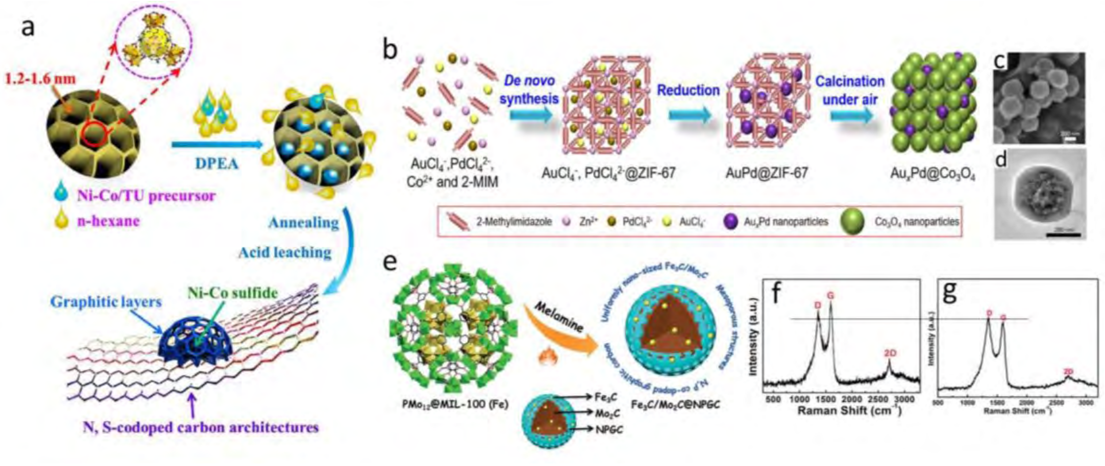

Fig. 8. a) Illustration of the preparation of mesoporous Ni-Co-S@G/NSC. Reproduced with permission.[15] Copyright 2017, Elsevier. b) *De Novo* synthesis of zeolitic imidazolate framework-67-derived Au-Pd embedded cobalt oxide cages. c) SEM image and d) TEM image of AuPd@ZIF-67 NPs. Reproduced with permission.[129] Copyright 2020, Elsevier. e) Preparation of the $Fe_3C/Mo_2C$@NPGC nanocomposite derived from POM-based MOFs. Raman spectroscopy f) of $Fe_3C/Mo_2C$@NPGC and g) $Fe_3C$@C. Reproduced with permission.[132] Copyright 2016, The Royal Society of Chemistry.

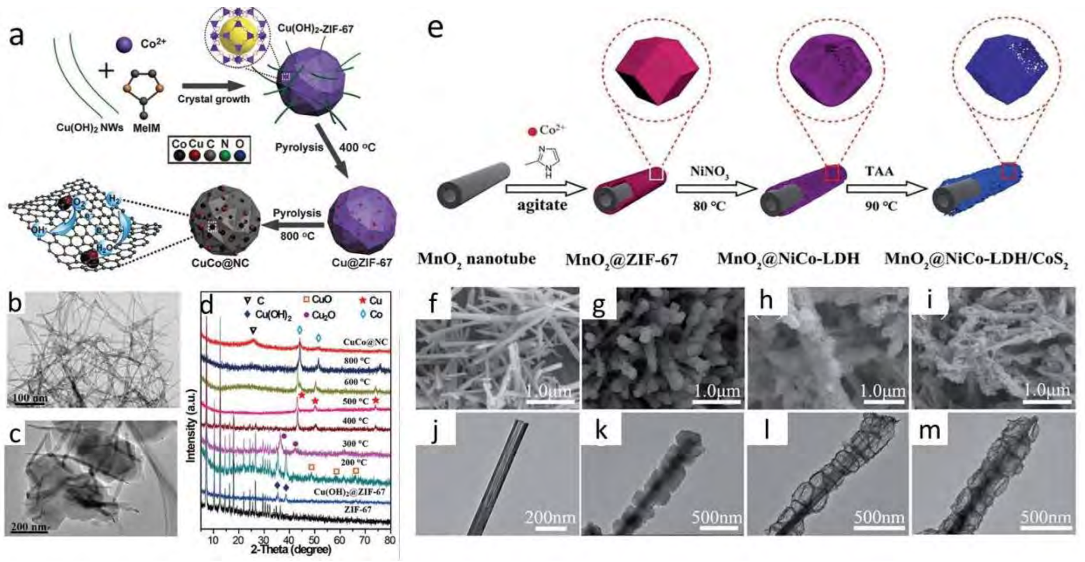

Fig. 9. a) Schematic representation of the synthesis process of CuCo@NC. TEM images of b) bare $Cu(OH)_2$ nanowires and c) ZIF-67 polyhedrons grown on $Cu(OH)_2$ nanowires. d) XRD patterns of ZIF-67, $Cu(OH)_2$@ZIF-67, $Cu(OH)_2$@ZIF-67 calcined at different temperatures, and CuCo@NC. Reproduced with permission.[145] Copyright 2017, WILEY VCH. e) Schematic diagram of the synthesis of $MnO_2$@Ni-Co LDH/$CoS_2$. SEM images and TEM images of (f, j) $MnO_2$, (g, k) $MnO_2$@ZIF-67, (h, l) $MnO_2$@NiCo-LDH and (i, m) $MnO_2$@NiCo-LDH/$CoS_2$. Reproduced with permission.[151] Copyright 2019, The Royal Society of Chemistry.

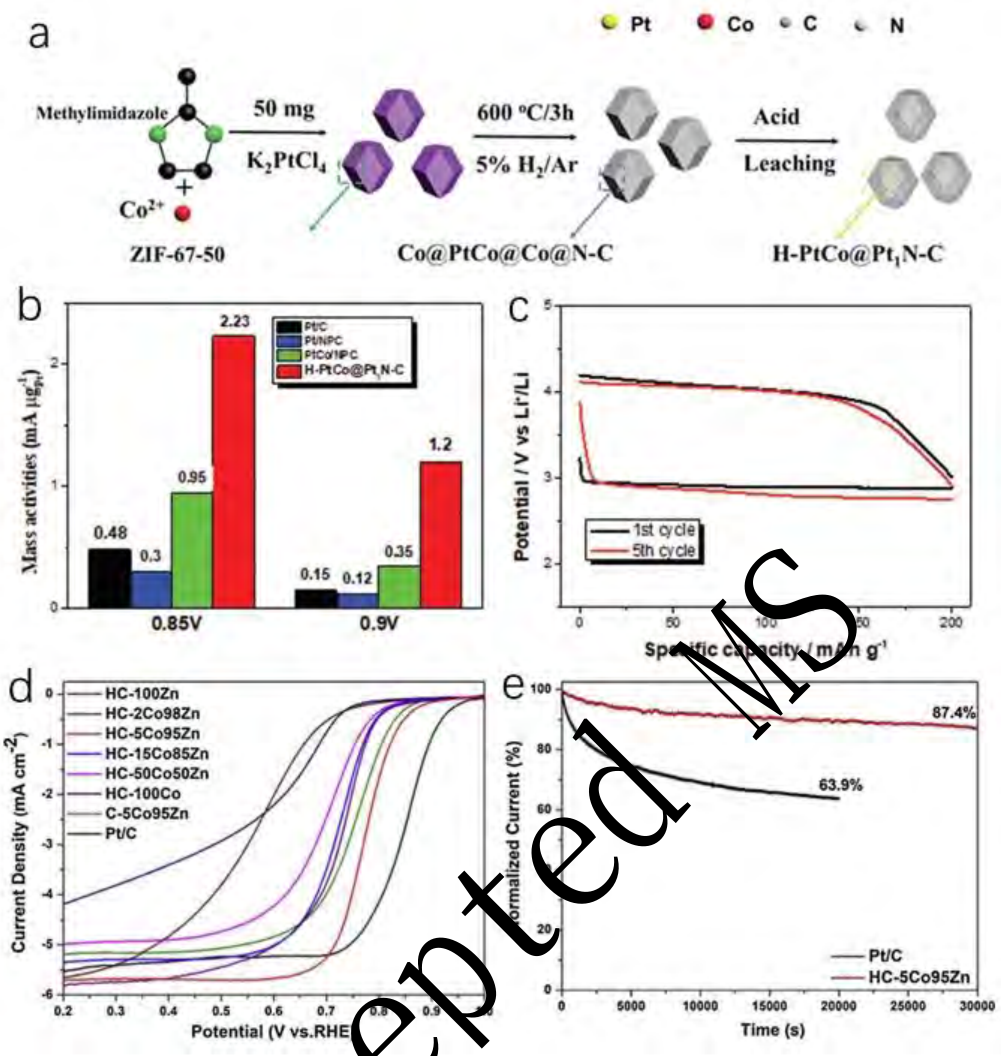

Fig. 10. a) Schematic illustration of the fabrication process for H-PtCo@Pt₁N-C. b) Comparison of mass activities for H-PtCo@Pt₁N-C, PtCo/NPC, Pt/NPC, and Pt/C at 0.85 and 0.9 V. c) Cycling stability of H-PtCo@Pt₁N-C in tetraethylene glycol dimethyl ether. Reproduced with permission.[164] Copyright 2019, WILEY VCH. d) LSV curves of the HC-xCo(100-x)Zn, C-5Co95Zn, and Pt/C for ORR in $O_2$-saturated 0.1 M $HClO_4$ at 1600 rpm. e) Chronoamperometric responses of Pt/C and HC-5Co95Zn in 0.1 M $HClO_4$. Reproduced with permission.[166] Copyright 2018, Elsevier.

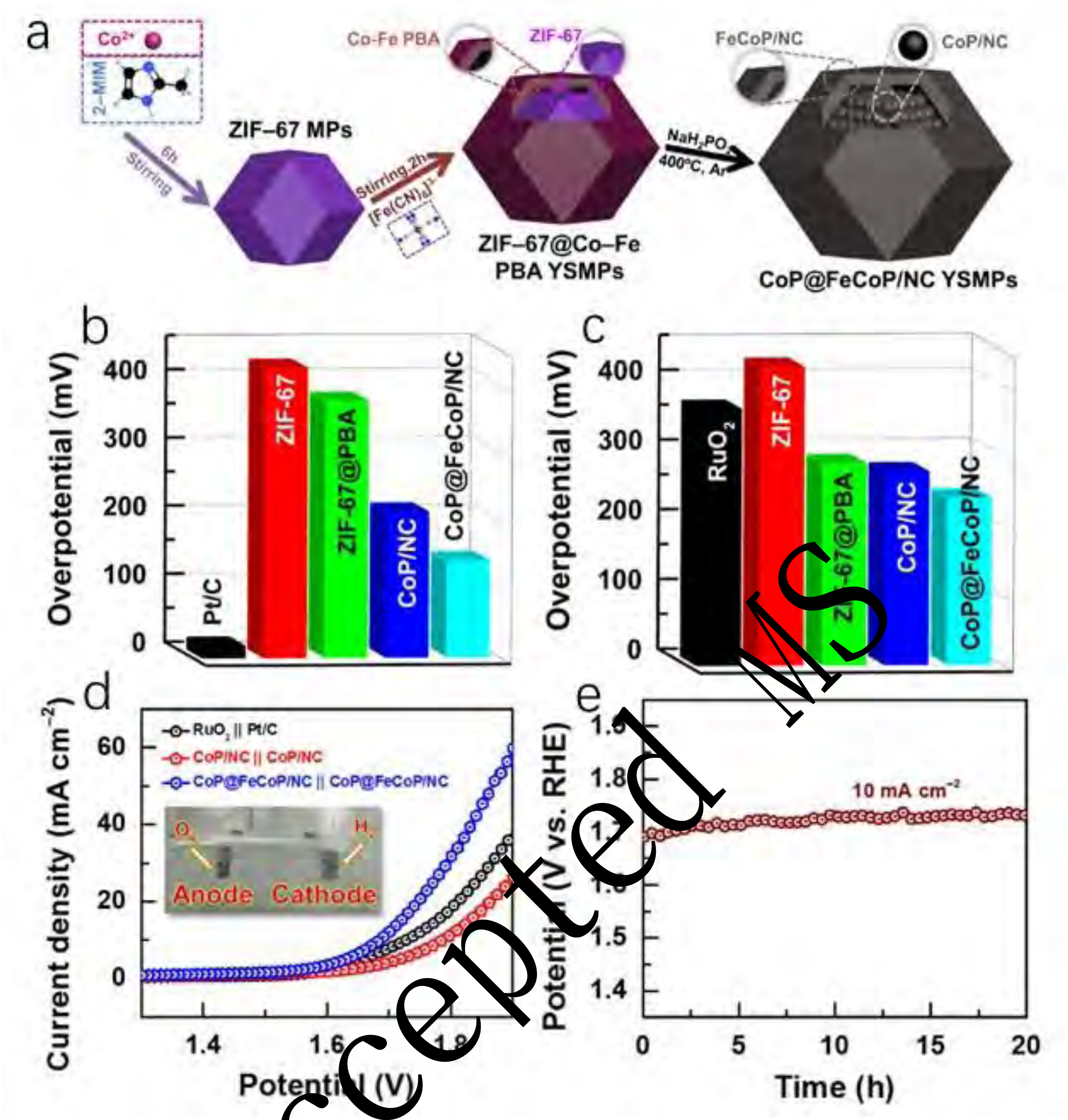

Fig. 11. a) Schematic illustration of the formation process of CoP@FeCoP/NC. b) Comparison of the overpotential of achieved a current density of 10 mA cm$^{-2}$ for HER. c) Comparison of the overpotential of achieved a current density of 10 mA cm$^{-2}$ for OER. d) Polarization curves of different catalysts for overall water splitting of the electrolyzer in alkaline. e) Stability test results of the electrolyzer powered by a single AA battery of CoP@FeCoP/NC||CoP@FeCoP/NC. Reproduced with permission.[192] Copyright 2020, Elsevier.

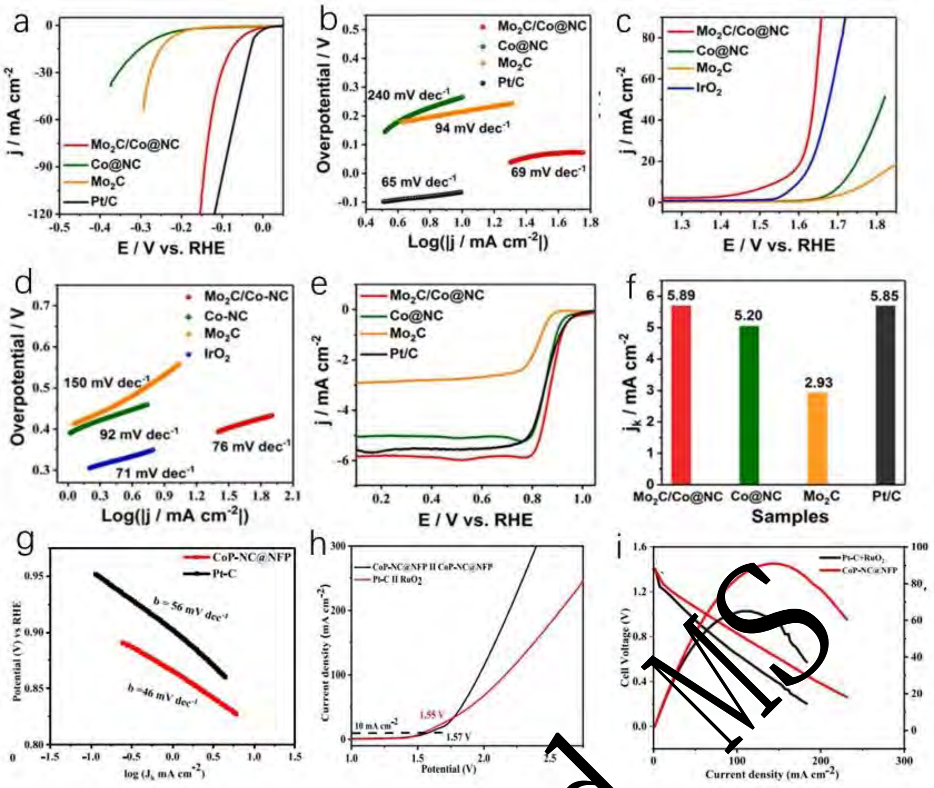

Fig. 12. HER performance of the electrocatalyst: a) LSV curves of the electrocatalysts at a scan rate of 5 mV s$^{-1}$ and (b) Tafel slope in 1 M KOH. OER performance of the electrocatalyst: c) LSV curves of the electrocatalysts at a scan rate of 5 mV s$^{-1}$ and (d) Tafel slope in 1 M KOH. ORR performance of the electrocatalyst: e) LSV curves of $Mo_2C$/Co@NC, Co@NC, $Mo_2C$ and Pt/C and f) the electrochemical activity given as the diffusion-limited current density ($J_L$) at 0.2 V (vs. RHE) for various electrocatalysts. Reproduced with permission.[198] Copyright 2021, Elsevier. g) Tafel slope of CoP-NC@NFP and Pt-C for ORR. h) LSV curves of CoP-NC@NFP||CoP-NC@NFP and Pt-C||$RuO_2$ water electrolysis device in 1.0 M KOH for overall water-splitting. i) Power density curve and discharge curves compared with the state-of-the-art catalyst Pt-C + $RuO_2$ for the zinc-air battery. Reproduced with permission.[199] Copyright 2021, Elsevier.

**Table 1.** Advantages and disadvantages of different strategies for fabricating multi-metallic nanomaterials from MOFs.

| Design strategies | Advantages | Disadvantages |
|---|---|---|
| Metal nodal substitution | (i) Facile and usual operation process;<br>(ii) Good preservation for original MOF structure;<br>(iii) Simple but effective modulation of metal content;<br>(iv) Easy to control nanoparticle size, shape and composition. | (i) Hard to incorporation of metal ions with different electronic configuration. |
| Seed epitaxial growth | (i) Beneficial to synthetic core-shell/hollow structure;<br>(ii) Integration individual advantages of different MOFs;<br>(iii) Tuning the solid nucleation. | (i) Strict requirements on similar topological structure between MOFs. |
| Ion-exchange strategy | (i) Energy-efficient;<br>(ii) Moderate reaction conditions;<br>(iii) Facile to obtain multiple shelled structures and multiple-component composites. | (i) Strict requirements on reaction time and substance concentration;<br>(ii) Possible structural distortion. |

| | | |
|---|---|---|
| Guest species encapsulation strategy | (i) Homogeneous distribution of metal NPs with uniform size;<br>(ii) Multi-spatial-compartmental nanoreactor. | (i) Highly dependent on pore size of MOFs;<br>(ii) Limited encapsulated amount. |
| Solution impregnation strategy | (i) Easily capture or anchor metal species;<br>(ii) Uniform growth of metal NPs on the inside and outside surface. | (i) Complex operation;<br>(ii) Possible structural collapse. |
| Combination with extraneous substrates | (i) Integration individual advantages of different materials;<br>(ii) Serving as secondary metal source and self-sacrificing templates;<br>(iii) Precise control MOFs on different substrates. | (i) Time-consuming process.<br>(ii) Complicated pre-synthetic process. |

**Table 2.** Summary of MOF-derived multi-metallic nanomaterials for electrocatalytic applications.

| MOF-derived multi-metallic nanomaterials | Precursors | Types of metals in the multi-metallic nanomaterials | Applications | Performances | Ref. |
|---|---|---|---|---|---|
| NiFe@C | NiFe–PBA | Alloy | OER | $\eta_{10\ \mathrm{mA\ cm}^{-2}}$ = 281 mV; Tafel slope = 53 mV decade$^{-1}$ | [223] |
| CoNiP | ZIF-67 | Phosphide | OER | $\eta_{10\ \mathrm{mA\ cm}^{-2}}$ = 209 mV; Tafel slope = 45 mV decade$^{-1}$ | [224] |
| $Ni_xCo_{3-x}O_{4-y}$ | ZIF-67 | Oxide | OER | $\eta_{10\ \mathrm{mA\ cm}^{-2}}$ = 320 mV; Tafel slope = 53 mV decade$^{-1}$ | [225] |
| NiCoP/C | ZIF-67 | Phosphide | OER | $\eta_{10\ \mathrm{mA\ cm}^{-2}}$ = 330 mV; Tafel slope = 96 mV decade$^{-1}$ | [178] |
| Zn–$CoSe_2$/CFC | Zn,Co–ZIF | Selenide | OER | $\eta_{10\ \mathrm{mA\ cm}^{-2}}$ = 356 mV; Tafel slope = 88 mV decade$^{-1}$ | [215] |
| FeNi@N-CNT | Zn/Fe/Ni–ZIF | Alloy | OER | $\eta_{10\ \mathrm{mA\ cm}^{-2}}$ = 300 mV; Tafel slope = 47.7 mV decade$^{-1}$ | [99] |
| Cu-Ni-$CoSe_x$ | Cu-Ni-Co PBA | Selenide | HER | $\eta_{10\ \mathrm{mA\ cm}^{-2}}$ = 50.2 mV; Tafel slope = 49.6 mV decade$^{-1}$ | [226] |
| Ni-Co-P-300 | Ni-Co PBA | Phosphide | HER | $\eta_{10\ \mathrm{mA\ cm}^{-2}}$ = 150 mV; Tafel slope = 60.6 mV decade$^{-1}$ | [227] |
| Fe-$Co_xP$ NCs | Fe-Co PBA | Phosphide | HER | $\eta_{10\ \mathrm{mA\ cm}^{-2}}$ = 125 mV; Tafel slope = 55 mV decade$^{-1}$ | [228] |
| NiFe-NGMT | Ni-MOF | Alloy | HER | $\eta_{10\ \mathrm{mA\ cm}^{-2}}$ = 70.5 mV; Tafel slope = 63.4 mV decade$^{-1}$ | [229] |
| PtFeCo@CN | Co-Fe PBA | Alloy | HER | $\eta_{10\ \mathrm{mA\ cm}^{-2}}$ = 45 mV; Tafel slope = 32 mV decade$^{-1}$ | [230] |
| CoFeZn@pCNT | Zn/Co–ZIF | Telluride | ORR | $E_{1/2}$ = 0.87 V vs RHE | [231] |
| Fe–Co alloy/N-doped carbon | ZIF-8/ZIF-67 | Alloy | ORR | $E_{1/2}$ = 0.88 V vs RHE; Tafel slope = 79 mV decade$^{-1}$ | [232] |
| CoFe@C | MET-6 | Atomically | ORR | $E_{1/2}$ = 0.89 V vs RHE; $E_{oneset}$ = 0.98 V vs RHE | [233] |

| | | | | | |
|---|---|---|---|---|---|
| | | dispersed Co–Fe | | | |
| A-CoPt-NC | Co-MOF | Atomically dispersed Co–Pt | ORR | $E_{1/2}$ = 0.96 V vs RHE; $E_{\mathrm{oneset}}$ = 0.93 V vs RHE ((Co-Pt)@N8V4) | [163] |
| Co–NiSe@C | ZIF-67 | Selenide | OER, HER | OER: $\eta_{30\ \mathrm{mA\ cm}^{-2}}$ = 275 mV; Tafel slope = 63 mV decade$^{-1}$<br>HER: $\eta_{10\ \mathrm{mA\ cm}^{-2}}$ = 90 mV; Tafel slope = 81 mV decade$^{-1}$ | [216] |
| Ni–Fe–P@C | Ni–Fe–MOF | Phosphide | OER, HER | OER: $\eta_{10\ \mathrm{mA\ cm}^{-2}}$ = 217 mV; Tafel slope = 40 mV decade$^{-1}$<br>HER: $\eta_{10\ \mathrm{mA\ cm}^{-2}}$ = 79 mV; Tafel slope = 92.6 mV decade$^{-1}$ | [234] |
| $Cu_{0.3}Co_{2.7}P$/NC | Co–Cu–ZIF | Phosphide | OER, HER | OER: $\eta_{10\ \mathrm{mA\ cm}^{-2}}$ = 190 mV; Tafel slope = 44 mV decade$^{-1}$<br>HER: $\eta_{10\ \mathrm{mA\ cm}^{-2}}$ = 220 mV; Tafel slope = 122 mV decade$^{-1}$ | [235] |
| CoFe@NC/KB-800 | Co-MOF | Alloy | OER, ORR | OER: $\eta_{10\ \mathrm{mA\ cm}^{-2}}$ = 385 mV; Tafel slope = 91 mV decade$^{-1}$<br>ORR: $E_{1/2}$ = 0.845 V vs RHE; $E_{\mathrm{oneset}}$ = 0.95 V vs RHE; Tafel slope = 88 mV decade$^{-1}$ | [236] |

| | | | | | |
|---|---|---|---|---|---|
| $Ni_{0.6}Fe_{0.4}$ CM | Ni-Fe MOF | Alloy | OER, ORR | OER: $\eta_{10\ mA\ cm^{-2}}$ = 320 mV; Tafel slope = 98.14 mV $decade^{-1}$<br>ORR: $E_{1/2}$ = 0.75 V vs RHE; $E_{onset}$ = 0.88 V vs RHE; Tafel slope = 103.81 mV $decade^{-1}$ | [237] |
| FeNiCo@NC-P | $Fe_2Ni$_MIL-88@ZnCo_ZIF | Alloy/Phosphide | OER, ORR | OER: $\eta_{10\ mA\ cm^{-2}}$ = 154 mV; Tafel slope = 64 mV $decade^{-1}$<br>ORR: $E_{1/2}$ = 0.84 V vs RHE; Tafel slope = 53 mV $decade^{-1}$ | [238] |
| CoP-NC@NiFeP | Co-MOF | Phosphide | OER, ORR, HER | OER: $\eta_{50\ mA\ cm^{-2}}$ = 270 mV; Tafel slope = 84 mV $decade^{-1}$<br>ORR: $E_{1/2}$ = 0.831 V vs RHE; Tafel slope = 46 mV $decade^{-1}$<br>HER: $\eta_{50\ mA\ cm^{-2}}$ = 163 mV; Tafel slope = 108 mV $decade^{-1}$ | [239] |
| Ni1Co4S@C | ZIF-67 | Sulfide | OER, ORR, HER | OER: $\eta_{10\ mA\ cm^{-2}}$ = 280 mV; Tafel slope = 64 mV $decade^{-1}$ (Ni1Co4S@C-1000)<br>ORR: $E_{1/2}$ = 0.60 V vs RHE (Ni1Co4S@C-1000)<br>HER: $\eta_{10\ mA\ cm^{-2}}$ = 247 mV (Ni1Co4S@C-800) | [240] |